



HAL
open science

Ultrafast Oxidation of a Tyrosine by Proton-Coupled Electron Transfer Promotes Light Activation of an Animal-like Cryptochrome

Fabien Lacombat, Agathe Espagne, Nadia Dozova, Pascal Plaza, Pavel Müller, Klaus Brettel, Sophie Franz-Badur, Lars-Oliver Essen

► **To cite this version:**

Fabien Lacombat, Agathe Espagne, Nadia Dozova, Pascal Plaza, Pavel Müller, et al.. Ultrafast Oxidation of a Tyrosine by Proton-Coupled Electron Transfer Promotes Light Activation of an Animal-like Cryptochrome. *Journal of the American Chemical Society*, 2019, 141 (34), pp.13394-13409. 10.1021/jacs.9b03680 . hal-02284305

HAL Id: hal-02284305

<https://hal.science/hal-02284305>

Submitted on 5 Nov 2019

HAL is a multi-disciplinary open access archive for the deposit and dissemination of scientific research documents, whether they are published or not. The documents may come from teaching and research institutions in France or abroad, or from public or private research centers.

L'archive ouverte pluridisciplinaire **HAL**, est destinée au dépôt et à la diffusion de documents scientifiques de niveau recherche, publiés ou non, émanant des établissements d'enseignement et de recherche français ou étrangers, des laboratoires publics ou privés.

Ultrafast Oxidation of a Tyrosine by Proton-Coupled Electron Transfer Promotes Light Activation of an Animal-like Cryptochrome

Fabien Lacombat, Agathe Espagne, nadia dozova, Pascal Plaza, Pavel Müller, Klaus Brettel, Sophie Franz-Badur, and Lars-Oliver Essen

J. Am. Chem. Soc., **Just Accepted Manuscript** • DOI: 10.1021/jacs.9b03680 • Publication Date (Web): 01 Aug 2019

Downloaded from pubs.acs.org on August 5, 2019

Just Accepted

“Just Accepted” manuscripts have been peer-reviewed and accepted for publication. They are posted online prior to technical editing, formatting for publication and author proofing. The American Chemical Society provides “Just Accepted” as a service to the research community to expedite the dissemination of scientific material as soon as possible after acceptance. “Just Accepted” manuscripts appear in full in PDF format accompanied by an HTML abstract. “Just Accepted” manuscripts have been fully peer reviewed, but should not be considered the official version of record. They are citable by the Digital Object Identifier (DOI®). “Just Accepted” is an optional service offered to authors. Therefore, the “Just Accepted” Web site may not include all articles that will be published in the journal. After a manuscript is technically edited and formatted, it will be removed from the “Just Accepted” Web site and published as an ASAP article. Note that technical editing may introduce minor changes to the manuscript text and/or graphics which could affect content, and all legal disclaimers and ethical guidelines that apply to the journal pertain. ACS cannot be held responsible for errors or consequences arising from the use of information contained in these “Just Accepted” manuscripts.

Ultrafast Oxidation of a Tyrosine by Proton-Coupled Electron Transfer Promotes Light Activation of an Animal-like Cryptochrome

Fabien Lacombat,^a Agathe Espagne,^a Nadia Dozova,^a Pascal Plaza,^{*,a} Pavel Müller,^{*,b} Klaus Brettel,^b Sophie Franz-Badur,^c Lars-Oliver Essen^{*,c}

^a PASTEUR, Département de chimie, École normale supérieure, PSL University, Sorbonne Université, CNRS, 75005 Paris, France. E-mail: pascal.plaza@ens.fr

^b Institute for Integrative Biology of the Cell (I2BC), CEA, CNRS, Univ. Paris-Sud, Université Paris-Saclay, 91198, Gif-sur-Yvette cedex, France. E-mail: pavel.muller@i2bc.paris-saclay.fr

^c Department of Chemistry, LOEWE Center for Synthetic Microbiology, Philipps University, 35032 Marburg, Germany. E-mail: essen@chemie.uni-marburg.de

ABSTRACT: The animal-like cryptochrome of *Chlamydomonas reinhardtii* (*CraCRY*) is a recently discovered photoreceptor that controls the transcriptional profile and sexual life cycle of this alga by both blue and red light. *CraCRY* has the uncommon feature of efficient formation and longevity of the semi-reduced neutral form of its FAD cofactor upon blue light illumination. Tyrosine Y₃₇₃ plays hereby a crucial role by elongating as fourth member the electron transfer (ET) chain that comprises the tryptophan triad otherwise found in most other cryptochromes and DNA photolyases. Here, we report the full mechanism of light-induced FADH[•] formation in *CraCRY* using transient absorption spectroscopy from hundreds of femtoseconds to seconds. Electron transfer starts from ultrafast reduction of excited FAD to FAD^{•-} by the proximal tryptophan (0.4 ps) and is followed by delocalized migration of the produced WH^{•+} radical along the tryptophan triad (3.7 and 55 ps). Oxidation of Y₃₇₃ by coupled ET to WH^{•+} and deprotonation then proceeds in ~800 ps, without any significant kinetic isotope effect, nor a pH effect between pH 6.5 and 9.0. The FAD^{•-}/Y₃₇₃[•] pair is formed with high quantum yield (~60%); its intrinsic decay by recombination is slow (~50 ms), favoring reduction of Y₃₇₃[•] by extrinsic agents and protonation of FAD^{•-} to form the long-lived, red-light absorbing FADH[•] species. Possible mechanisms of tyrosine oxidation by ultrafast proton-coupled ET in *CraCRY*, a process about 40 times faster than the archetypal tyrosine-Z oxidation in photosystem II, are discussed in detail.

1. INTRODUCTION

Cryptochrome blue-light receptors are responsible for various biological photoinduced responses, such as plant photomorphogenesis, circadian rhythm entrainment in animals or presumably magnetoreception in migrating birds.¹⁻⁴ The triggering mechanism of cryptochromes is based on the photoreduction of their flavin cofactor (FAD: flavin adenine dinucleotide), in a very similar way as in the so-called photoactivation reaction of photolyases, a group of closely related enzymes able to photorepair UV-damaged DNA.^{1,5-8} Some bifunctional cryptochromes even act both as light receptors and DNA-repairing enzymes.⁹⁻¹⁴ The evolutionary links between the different members of the photolyase and cryptochrome superfamily (PCSf) may be found in various reports.¹⁵⁻¹⁹

A new type of cryptochrome was recently discovered in the green alga *Chlamydomonas reinhardtii*, exhibiting homology to animal but not plant cryptochromes, called animal-like cryptochrome (the *C. reinhardtii* protein is noted *CraCRY*). In contrast to other cryptochromes, *CraCRY* appears to be capable of inducing a genetic response not only to blue, but also to red light.²⁰⁻²² This feature is probably related to another unique property of *CraCRY*, the very efficient formation and stabilization of its semi-reduced (red light-absorbing) flavin cofactor (FADH•) that can be easily accumulated under blue light illumination and lives for seconds to minutes (depending on pH).^{20,23} This process relies on the oxidation of the phenolic moiety of the tyrosine residue Y₃₇₃ as its mutation to phenylalanine abolishes this effect.²⁴ Y₃₇₃ is located at the distal end of the "canonical" tryptophan triad (W₃₉₉, W₃₇₆ and W₃₂₂ in *CraCRY*; see Figure 1A) that is conserved in most members of the PCSf –except the subfamilies of bacterial (6-4) photolyases and class II photolyases – and is involved in the photoreduction of FAD.^{3,7,25} In the canonical PCSf members, the excited flavin abstracts an electron from a nearby (proximal) tryptophan, which gets in turn reduced by a second (medial) tryptophan, before being reduced by a third (distal) one. The distal tryptophan is usually surface-exposed and can hence be reduced by external electron donors such as thiol compounds²⁶ or NAD(P)H.^{27,28} For animal-like cryptochromes and (6-4) photolyases, a fourth aromatic residue, Y₃₇₃ in *CraCRY* and W₃₆₀ in the (6-4) photolyase from *Xenopus laevis*, has been found to act as final electron donor of an extended electron transfer chain.^{24,29-32}

Transient absorption spectroscopy (TAS) has been extensively used to study the mechanistic details of the photoreduction of photolyases^{31,33-40} and cryptochromes, taking advantage of the rather distinct absorption spectra of the species involved (Figure 1B).^{35,39,41} Ultrafast TAS studies have in particular shown that when the flavin is initially oxidized (FAD_{ox}), the primary electron transfer (ET) takes place in less than one picosecond,^{31,35,37,39,41} producing a radical pair of reduced flavin (FAD•⁻) and oxidized

1
2
3 tryptophan ($\text{WH}^{\bullet+}$)[†]. Slower steps observed in the ps regime were assigned to the migration of the
4 electron hole along the tryptophan triad, which competes with partial charge recombination of the
5 radical pairs. The distal $\text{WH}^{\bullet+}$ typically deprotonates in a few hundred nanoseconds, forming the neutral
6 W^{\bullet} radical.^{33,42} Besides the tryptophan triad, Liu *et al.*³⁷ demonstrated for the class I CPD photolyase of
7 *E. coli* (*EcCPDI*) the involvement of two tryptophans acting as branch lines: one weakly competes with
8 the proximal tryptophan for the reduction of the excited flavin, the other temporarily competes with the
9 medial tryptophan for the reduction of the proximal $\text{WH}^{\bullet+}$ cation. Counterparts of these branch
10 tryptophans are also present in *CraCRY*, *i.e.* W_{401} and W_{332} (shown in gray in Figure 1A). Ultrafast TAS had
11 not yet been applied to *CraCRY* and the few studies using "classical" TAS^{24,29} were essentially limited to
12 timescales above 1 μs .
13
14

15
16
17
18
19
20 Transient EPR data by Nohr *et al.*²⁹ on oxidized *CraCRY* on the μs timescale have shown that fast,
21 unresolved, joint oxidation and deprotonation of Y_{373} occurs upon excitation of the flavin. In the same
22 study, monitoring the decay of $\text{FAD}^{\bullet-}$ by transient absorption yielded a lifetime of 26 ms that was
23 attributed to recombination of the radical pair $\text{FAD}^{\bullet-}/\text{Y}^{\bullet\ddagger}$.²⁹ A transient absorption study by Oldemeyer
24 *et al.*²⁴ using semi-reduced *CraCRY* (containing FADH^{\bullet}) prepared by pre-illumination with blue light also
25 demonstrates oxidation of a tyrosyl residue, in "less than 1 μs ", and reports the decay of the
26 corresponding $\text{FADH}^{\bullet}/\text{Y}^{\bullet}$ pair in 2.6 s. Much slower and only partial oxidation of tyrosyl residues was
27 reported previously during photoreduction of some members of the PCSf: time constants of $\sim 70 \mu\text{s}$ for
28 the photolyase from *A. nidulans*,⁴³ $\sim 1.5 \text{ ms}$ for cryptochrome 1 from *A. thaliana*⁴⁴ and $\sim 1 \text{ ms}$ for the CPD
29 class II photolyase from *M. mazei*.⁴⁵
30
31
32
33
34
35

36
37 Oxidation and back-reduction of tyrosyl residues has been discovered to be involved in the
38 functioning of several enzymes, like prostaglandin H synthase, galactose oxidase, ribonucleotide
39 reductase or photosystem II (PSII).⁴⁶ The case of PSII is of particular importance because the possibility
40 to trigger the reactions by light allowed for detailed time-resolved studies of the reaction mechanism
41 and is still a matter of discussion.⁴⁷⁻⁵³ The one-electron reduction potential of tyrosine ($\text{YH}^{\bullet+}/\text{YH}$ couple)
42 is as high as $\sim 1.35 \text{ V}$ (vs NHE) in aqueous solution.⁵⁴ However, the oxidant of tyrosine in PSII, the
43 chlorophyll cation P680^+ , provides only $\sim 1.25 \text{ V}$,⁵⁵ so that a simple ET from YH to P680^+ would be uphill
44 (endergonic). Nevertheless, tyrosine oxidation by P680^+ can be as fast as $\sim 30 \text{ ns}$.⁵⁶⁻⁵⁹ In fact, the $\text{YH}^{\bullet+}$
45
46
47
48
49
50
51
52

53
54 [†] The notation $\text{WH}^{\bullet+}$ indicates the protonated tryptophanyl radical, while W^{\bullet} refers to the deprotonated radical.

55 [‡] Y^{\bullet} stands for the deprotonated tyrosyl radical; the corresponding protonated species is noted $\text{YH}^{\bullet+}$.
56
57
58
59
60

1
2
3 radical is strongly acidic ($pK_a \sim -2$),⁶⁰ so when ET is coupled to deprotonation of $YH^{*\dagger}$, the overall
4 reaction is well downhill, *i.e.* exergonic.
5

6 Another case of light-induced tyrosine oxidation was more recently discovered in BLUF (blue-light
7 sensing using FAD) photoreceptor proteins.⁶¹⁻⁶³ In the dark-adapted Slr 1694 BLUF, ultrafast (tens of
8 picoseconds) ET from Y_8 to the photoexcited FAD cofactor and similarly fast PT from $Y_8H^{*\dagger}$ to $FAD^{\bullet-}$ via a
9 glutamine residue yield an $Y_8^{\bullet}/FADH^{\bullet}$ radical pair.^{61,62} This pair recombines on a 100-ps timescale, but
10 rearrangements of the hydrogen bond network (and a related red shift of the FAD absorption spectrum)
11 persist for seconds and represent the signaling state of the photoreceptor. In the light-adapted Slr 1694
12 BLUF, formation the of $Y_8^{\bullet}/FADH^{\bullet}$ pair is even faster (~ 1 ps), by concerted proton-coupled electron
13 transfer.⁶³
14
15
16
17
18
19

20 Proton-coupled electron transfer (PCET) has been the subject of intense theoretical work and
21 experimental studies in chemistry and biology because of its crucial role in avoiding high energy
22 intermediates in chemical and enzymatic catalysis, notably for solar energy conversion.⁶⁴⁻⁶⁹ As
23 summarized by Hammes-Schiffer and Stuchebrukhov,⁶⁴ two types of coupled reactions can be
24 distinguished. In concerted electron and proton transfer (PT) reactions, both ET and PT occur in one
25 step.⁶³ In sequential reactions, the transitions occur in two steps: ET followed by PT (noted ET/PT) or PT
26 followed by ET (PT/ET). In both cases, the first step is typically uphill in energy and the second step is
27 downhill to the final product state. Tyrosine oxidation in the BLUF domain may constitute an exception,
28 which is commented further at the end of Section 4.2.2. A hallmark of a concerted PCET reaction is the
29 observation of a substantial normal kinetic isotope effect (KIE), *i.e.* the reaction is slowed down when
30 the transferred proton is replaced by a deuteron. Sequential ET/PT and PT/ET typically show a (normal)
31 KIE only when PT becomes rate limiting.
32
33
34
35
36
37
38
39

40 The absence of a KIE on the oxidation of tyrosine in PSII in ~ 30 ns may point to a sequential PT/ET,
41 where the hydroxyl proton of the tyrosine moves to a nearby histidine residue prior to rate-limiting
42 ET.^{50,53} A slower (few μ s) tyrosine oxidation in PSII depleted of the oxygen-evolving complex, however,
43 showed a normal KIE and was hence assigned to concerted PCET.⁴⁹
44
45
46

47 The presumed oxidant of tyrosine in *CraCRY*, namely $W_{322}H^{*\dagger}$, is likely to have an even lower
48 reduction potential (1.07 V for the $WH^{*\dagger}/WH$ couple in aqueous solution⁵⁴) than $P680^+$ in PSII, suggesting
49 that tyrosine oxidation in *CraCRY* occurs by some type of PCET as well. The main objective of the present
50 work was to resolve the kinetics of tyrosine oxidation in *CraCRY* and to contribute to establishing its
51 reaction mechanism. Ultrafast pump-probe and real-time transient absorption spectroscopy on
52 timescales from hundreds of fs to hundreds of ms were used to monitor the complete reaction
53
54
55
56
57
58
59
60

1
2
3 sequence of flavin photoreduction. Wild-type (WT) *CraCRY* was compared to its Y373F mutant.[§] This
4 mutation was expected to ablate the electron donor character of Y₃₇₃ and enable us to distinguish
5 reactions involving Y₃₇₃ from preceding reactions that should not be significantly affected by the
6 mutation.
7
8
9

10 11 **2. MATERIALS AND METHODS**

12 13 14 **2.1 Sample preparation**

15
16 The *Chlamydomonas reinhardtii* animal-like cryptochrome (*CraCRY*) samples were prepared as recently
17 described.⁷⁰
18

19
20 For transient absorption experiments, we used a 50 mM phosphate buffer at pH 8.4, containing 100
21 mM NaCl and 20% glycerol. The D₂O buffer was composed of heavy water (99.9 atom % D, Sigma-
22 Aldrich) and D₂O-exchanged glycerol (10% v/v glycerol in D₂O, dried in a rotary evaporator; procedure
23 repeated twice). Some samples had to be concentrated with centrifugal concentrators (Vivaspin 500,
24 Sartorius or Amicon Ultra-4, Sigma-Aldrich; molecular weight cutoff: 30 kDa) to achieve suitable optical
25 densities. Prior to the experiments, *CraCRY* solutions were passed through a gel-filtration column (Micro
26 Bio-Spin6, BioRad), equilibrated with the working buffer, to eliminate unbound FAD. The steady-state
27 absorption spectra of *CraCRY* samples used for femtosecond transient absorption spectroscopy are
28 shown in SI, Section S1 (Figure S1).
29
30
31
32
33
34
35

36 **2.2 Femtosecond Transient Absorption Spectroscopy (TAS)**

37 38 **2.2.1 Setup**

39
40 Polarized transient absorption anisotropy was here used to both access the transient population
41 dynamics, through the isotropic transient absorption, and probe orientation of the transient species
42 with the associated transient absorption anisotropy. Anisotropy is indeed particularly useful to help
43 distinguishing the different WH^{•+} radicals involved in the photoreduction process, as was previously
44 done for other photolyases and cryptochromes.^{31,40,41,71} The pump-probe setup, with white-light
45 continuum probe, has been previously described.^{31,39,40} The pump beam was tuned at 475 nm. By
46 comparison with a reference sample of tris-(2,2'-bipyridyl)-ruthenium(II) complex,^{72**} it was checked
47
48
49
50
51
52
53

54 [§] The abridged notations WT and Y373Y will be used to refer to these variants.

55 ^{**} Systematic measurements on the [Ru(bpy)₃]²⁺ complex were also used to (i) ensure that no major alteration of
56 the transient spectra occurred upon varying the pump-probe delay over the 3.2-ns range of an optical delay line,
57
58
59

1
2
3 that the fraction of excited molecules in the probed volume was about 3% (case of WT in H₂O buffer),
4 which lies in the linear regime.
5

6 In order to avoid probing the same region consecutively, the sample cuvette (1-mm optical
7 path) was continuously moved back and forth in horizontal and vertical directions, each pump
8 shot irradiating an area of the order of 0.01 mm². A relatively large volume (~250 μL in a 10-mm wide
9 cell) of sample was used for the experiment with WT-*CraCRY* in H₂O buffer. Alternatively, four smaller
10 cells (2-mm wide, containing ~60 μL) were used for WT in D₂O buffer, each one being irradiated
11 for a shorter time while the others were recovering in the dark. One 60-μL cell was sufficient for
12 Y373F since FADH• does not accumulate so easily in this *CraCRY* mutant.^{24,29} Steady-state
13 absorption spectra of the samples were regularly recorded during the experiments to check that no
14 significant accumulation of FADH• or sample degradation occurred. All experiments were performed at
15 room temperature (20 °C).
16
17
18
19
20
21
22

23 2.2.2 Data analysis

24 The polarized differential absorption spectra (ΔA_{\parallel} and ΔA_{\perp}), obtained from the transmitted probe
25 beam intensities, were first corrected from the chirp of the probe beam, which was independently
26 measured by recording cross-phase modulation⁷³ (XPM) in the pure solvent. These raw polarized spectra
27 were transformed into isotropic transient absorption spectra (ΔA_{iso}) and transient anisotropy spectra (r)
28 using Equations 1 and 2. Scattering of the pump beam was masked in the spectra, both for data analysis
29 and figure presentation.
30
31
32
33
34

$$\begin{cases} \Delta A_{iso} = \frac{1}{3}(\Delta A_{\parallel} + 2 \Delta A_{\perp}) & \text{(Eq. 1)} \\ r = \frac{\Delta A_{\parallel} - \Delta A_{\perp}}{\Delta A_{\parallel} + 2 \Delta A_{\perp}} & \text{(Eq. 2)} \end{cases}$$

35
36
37
38
39
40 Notably, the transient absorption spectra of WT samples displayed a weak signal at negative time
41 delays. This signal is due to a long-lived photoproduct (FAD•⁻/Y• pair²⁹) produced by the preceding pump
42 pulse (3 ms before the probe only shot and 6 ms before pump and probe shot), but still detectable
43 because the 2D movement imposed on the sample cell was not fast enough to regenerate entirely the
44 probed sample volume between two probe pulses. This spurious signal has been averaged, smoothed,
45 and subtracted from the raw transient absorption data. The resulting spectra are presented here.
46
47
48

49 Multiexponential global analysis was performed simultaneously on the parallel and perpendicular
50 data as previously described.^{31,39,40} Effective fits of the isotropic and anisotropy data were derived from
51
52
53

54
55 and (ii) make experiments recorded on different days spectrally comparable (minor corrections based on the
56 [Ru(bpy)₃]²⁺ complex spectra were applied).
57
58
59
60

1
2
3 the root fits with Equations 1 and 2. The time constants of the fits will be presented in Table 1 and the
4 corresponding isotropic decay-associated spectra (DADS) provided for reference in SI, Section 4.4 (Figure
5 S10). The global fits are however here more conveniently summarized by the evolution-associated
6 difference spectra (EADS), which correspond to a virtual cascading model with unit quantum yield
7 between state i and state $i + 1$ and increasing lifetimes.⁷⁴ The polarized EADS were in turn converted into
8 isotropic EADS and evolution-associated anisotropy spectra (EAAS) using Equations 1 and 2.
9

10
11
12
13 Spectral analysis of some isotropic EADS were performed as previously described.⁴⁰ The aim is to fit
14 the spectra by a Beer-Lambert sum of contributions from different species (FAD_{ox} , $\text{FAD}^{\bullet-}$, $\text{WH}^{\bullet+}$, Y^{\bullet}), the
15 spectra of which are taken from literature (see Figure 1B and SI, Section S5.1). To improve the quality of
16 the fits, the reference spectra were modified with two intertwined parameters, a shift s and a scaling
17 factor u , so that spectrum $\epsilon(\lambda)$ becomes $\epsilon'(\lambda) = \epsilon(u(\lambda-s))$. To avoid ambiguities coming from the overlap
18 of reference spectra, fits were preferred where the number of species in the sum could be kept low. In
19 particular, we focused on the difference between consecutive spectra, as follows: EADS_{i+1} was fitted
20 with EADS_i as a first fit component, multiplied by an adjustable factor (ϕ) understood as the yield of the
21 $i \rightarrow i + 1$ phase, plus additional components reflecting composition changes taking place during this
22 step.
23
24
25
26
27
28
29
30

31 2.3 Real-time TAS

32
33 Transient absorption kinetics on nanosecond to millisecond timescales were measured on two different
34 setups described in detail elsewhere.^{42,75,76} In experiments on the sub-ns/ns timescales, the samples
35 were excited at 355 nm by a Nd:YAG laser (Continuum Leopard SS-10, pulse duration of 100 ps,
36 repetition rate 2 Hz, and pulse energy in the order of ~ 2 mJ per cm^2). In all other experiments, the
37 samples were excited at 475 nm by a Nd:YAG-pumped optical parametric oscillator (OPO; Brilliant
38 B/Rainbow, Quantel, France, pulse duration of 5 ns, repetition rate 2 Hz or single flashes, and energy in
39 the order of ~ 5 mJ per cm^2). Laser energies were estimated from the amplitudes of signals obtained with
40 the $[\text{Ru}(\text{bpy})_3]\text{Cl}_2$ actinometer⁷⁷ under otherwise identical conditions and geometry.
41
42
43
44
45
46

47 Monitoring light was provided by continuous-wave lasers listed previously.⁷⁶ $2 \times 2 \times 10$ mm cells were
48 used (excitation pulses entered the sample through the 2×10 mm window; monitoring light through the
49 2×2 mm window). The monitoring light beams were attenuated by neutral density filters and, for the
50 experiments on ns to μs timescales, were mechanically chopped to produce rectangular light pulses of
51 $140 \mu\text{s}$ duration and energy in the order of $1 \mu\text{J}$ at the entrance of the cell, thus avoiding significant
52
53
54
55
56
57
58
59
60

1
2
3 actinic effects. These pulses were synchronized with the excitation laser flash (see Ref. ⁷⁵ for more
4 details).
5

6 Signals on the sub-ns/ns timescales were recorded using the Alphas UPD-200-UP photodiode (rise
7 time <175 ps; sensitive area 0.1 mm²; bandwidth 2 GHz), connected directly to the Infiniium 81004B
8 digital oscilloscope (from Agilent; bandwidth 10 GHz). Signals on the ns/ μ s timescales were recorded
9 using the Alphas UPD-500-UP photodiode (rise time <500 ps; sensitive area 0.5 mm²; bandwidth 600
10 MHz), connected via the Femto HCA electronic signal amplifier (DC-325 MHz, 28 dB) to a the Tektronix
11 DSA602A digital oscilloscope with bandwidth limit set to 100 MHz. Signals on the ms/s timescales were
12 amplified by the AM502 differential amplifier (Tektronix) with a bandwidth limited to 100 kHz.
13
14
15
16
17

18 All experiments were carried out at room temperature (~25 °C) and the concentration of both WT
19 and Y373F proteins in most experiments was ~60 μ M. Only for experiments on the ns timescale, a
20 higher concentrated (~110 μ M) WT sample was used in order to improve the signal-to-noise ratio (at all
21 wavelengths except 457 nm).
22
23
24
25
26

27 3. RESULTS

28 3.1 Femtosecond TAS

29 3.1.1 Isotropic spectral dynamics

30
31
32 The transient absorption spectra of WT-CraCRY, both WT and Y373F mutant, recorded between 300 fs
33 and 3.2 ns after excitation at 475 nm, are presented in Figure S4 of SI, Section S3.1, together with a
34 detailed description of them. In brief, at early pump-probe delays of (*e.g.* 300 fs), one recognizes the
35 typical features of excited FAD_{ox} (FAD_{ox}^{*}), with a bleaching band at 447 nm, stimulated emission (SE) at
36 538 nm and excited-state absorption (ESA) bands around 366, 507 nm and over 570 nm. The following
37 evolution may approximately be divided into three phases. From 0.3 to ~2 ps (Figure S4A), the SE band
38 decays and is substituted by a broad positive band, peaking around 600 nm. The changes in this phase
39 resemble closely those observed in several oxidized PCSf members and attributed to primary charge
40 separation forming a FAD^{•-}/WH^{•+} pair.^{31,39-41} Between ~2 and ~230 ps (Figure S4B), all bands decay
41 partially without much change of their shape, indicating some loss of FAD^{•-}/WH^{•+} pairs by charge
42 recombination. Between ~230 and 3200 ps (Figure S4C), all bands go on decaying partially but one
43 observes that the transient absorption band at around 600 nm decays to much greater extent and
44 becomes increasingly flatter, consistent with data obtained by real-time TAS and tentatively assigned to
45
46
47
48
49
50
51
52
53
54
55
56
57
58
59
60

1
2
3 reduction of WH^{*+} by Y_{373} (see Section 3.2). The evolution of the transient absorption spectra of WT-
4 CraCRY measured in deuterated buffer is essentially identical (SI, Section S3.2).
5

6
7 The Y373F mutant (Figure 2D-F) behaves very similarly to the WT as far as the first phase is
8 concerned but exhibits substantial differences afterwards. Firstly, the amplitude of the decay during the
9 second phase is much smaller than for WT and, secondly, the third phase is almost absent; only a very
10 weak decay of all bands without shape alteration occurs between 80 ps and 3.2 ns.
11
12

13 3.1.2 Kinetic analysis

14
15 All polarized transient absorption spectra of CraCRY could be globally fitted with a sum of 4
16 exponential components and a plateau. Table 1 summarizes the obtained time constants (with errors of
17 fit corresponding to a confidence interval of 95%). An illustration of the quality of such fits may be found
18 in SI, Section S4.1, with selected kinetic traces of both isotropic transient absorption and transient
19 anisotropy of WT in H_2O .
20
21
22
23

24 Figure 2 (A,C) shows the isotropic EADS of WT and Y373F in H_2O buffer (for WT in D_2O see SI, Section
25 S4.2). The evolution phases qualitatively sketched in Section 3.1.1 are here more precisely defined. The
26 initial excited-state decay occurs in about 0.4 ps for both WT and Y373F. The second phase is divided
27 into two kinetic steps, characterized by time constants of 3.7 and 55 ps for WT (4.9 and 56 ps in D_2O),
28 and 3.4 and 41 ps for Y373F. These time constants are similar in all cases but the amplitude associated
29 to the 41-ps decay of Y373F is, in relative value, smaller than that of the 55-ps decay of WT (Figure
30 2A,C). As mentioned above, the fourth decay of WT in 710 ps, with conspicuous flattening of the 600 nm
31 band and decay below 350 nm, is almost absent in Y373F. One observes instead a very small homothetic
32 decrease of all bands, in 630 ps. Figure 3 displays the EADS2-5 of WT and Y373F (H_2O buffer), normalized
33 at the maximum of the bleaching band (NEADS). This normalization approximately compensates for the
34 transient absorption losses due to the recovery of the initial state by charge recombination. Figure S9
35 (SI, Section S4.3) presents the same data in one-to-one comparison of the NEADS of WT and Y373F. The
36 effect of the Y373F mutation is clearly seen in those figures to block the prominent spectral changes
37 (decay of the absorption bands around 600 nm and 340 nm, relative absorption increase in the 390-
38 430-nm range), observed in WT during the EADS4→EADS5 kinetic step. Minor changes consisting
39 essentially of a small decay of the broad band around 600 nm observed during the EADS3→EADS4 step
40 in the WT are also blocked by the Y_{373} mutation.
41
42
43
44
45
46
47
48
49
50
51
52
53
54
55
56
57
58
59
60

3.1.3 Transient anisotropy

The raw transient anisotropy spectra are provided for reference in SI, Section S3. The evolution-associated anisotropy spectra (EAAS) deduced from the global analysis procedure are shown in Figure 2 (B, D) for WT in H₂O and in Figure S8B for WT in D₂O buffer. In brief, the four kinetic phases described above can also be clearly distinguished according to their anisotropy. The initial phase is characterized by very large changes between 500 and 650 nm, due to the decay of SE. Subsequently, and starting with the simpler case of Y373F, one observes marked changes between 330 and 375 nm as well as between *ca.* 510 and 650 nm, during the 2nd and 3rd steps. The last kinetic step is accompanied by minimal alterations of the anisotropy. In the case of WT, the anisotropy changes during the 2nd step are similar to those of Y373F but differences start to appear during the 3rd step; The marked decay around 510 nm in Y373F is in particular significantly smaller in WT. During the last kinetic step, an increase is observed for WT at this wavelength while no change occurs in Y373F. The final anisotropy spectrum of WT becomes very noisy above ~700 nm and below 350 nm because the corresponding isotropic spectrum (denominator in Equation 2) approaches here zero value. These regions have been masked in Figure 2 (B,D).

3.2 Real-time TAS

3.2.1 Sub-nanosecond to nanosecond timescale

To monitor the photoreactions of *CraCRY* on the sub-ns to ns timescale, we used a sub-ns TAS setup (see Section 2.3) with excitation pulses at 355 nm (*i.e.* in the near UV absorption band of FAD_{ox}). Signals recorded at representative wavelengths for WT *CraCRY* and its Y373F mutant are shown in Figure 4A and 4B, respectively (for other wavelengths, see Figures S2A and S3A). 405 nm in particular lies close to the expected absorption maximum of the Y• radical (see Figure 1B); note that a strong absorption increase due to FAD reduction from FAD_{ox} to FAD•⁻ is also expected at this wavelength. 457 nm is close to the absorption maximum of FAD_{ox} in the blue in order to monitor the negative absorption changes (bleaching) due to the reduction of FAD_{ox} to FAD•⁻; note that tyrosine and tryptophan radicals exhibit very weak absorptions at this wavelength so their contributions to the signal are expected to be minor compared to those associated with the redox state changes of FAD. At 488 nm, the neutral W• typically absorbs much stronger (~ 2.5 ×) than the protonated WH•⁺ (see Figure 1B). And finally at 562 nm, where essentially only the tryptophan radicals contribute, the opposite is the case – the molar absorption coefficient of the WH•⁺ radical is much higher (~ 3 ×) than that of the W• radical (see Figure 1B).

1
2
3 For the Y373F mutant (Figure 4B), the high-time-resolution signals show essentially only a very slight
4 decline (that will be resolved on a longer timescale, see Section 3.2.2). For the WT, however, one
5 observes prominent kinetic features already on the ns timescale (Figure 4A). In particular, at 562 nm
6 (red trace in Figure 4A), the signal exhibits a major decay from an initial level comparable to that in the
7 Y373F mutant (when corrected for concentration difference) to ~20% of its initial amplitude within a
8 few nanoseconds. Similar signals were observed at 515, 594 and 639 nm (Figure S2A), strongly
9 suggesting that they represent disappearance of a $WH^{\bullet+}$ radical (see the absorption spectrum of $WH^{\bullet+}$ in
10 Figure 1B). A global fit of all signals (at all measured wavelengths) with two shared time constants (using
11 Equation S1) yielded $\tau_1 = 550$ ps and $\tau_2 = 5.6$ ns at an amplitude ratio of approx. 3:1 for signals at 515 nm
12 and above (see Figure S2B). The 550 ps phase may contain contributions from even faster processes that
13 could not be resolved at the instrumental time resolution of 300 ps (see above for data obtained by
14 ultrafast spectroscopy).

15
16 A priori, disappearance of the $WH^{\bullet+}$ signature in WT *CraCRY* could be not only caused by the
17 expected ET from Y_{373} but also due to back ET from $FAD^{\bullet-}$ or to deprotonation. Deprotonation of $WH^{\bullet+}$
18 would form the neutral radical W^{\bullet} and should be accompanied by an absorption increase at 488 nm (as
19 observed in the Y373F mutant; see Figure S3B). Instead, the disappearance of $WH^{\bullet+}$ within a few
20 nanoseconds in WT *CraCRY* was accompanied by bleaching at 488 nm (green trace in Figure 4A),
21 excluding deprotonation as major process. Back ET from $FAD^{\bullet-}$ to $WH^{\bullet+}$ should be accompanied by
22 recovery of the bleaching of the absorption band of FAD_{ox} around 450 nm. A partial recovery in approx.
23 1 ns was indeed observed at 457 nm (blue trace in Figure 4A), but represents only ~20% of the initial
24 bleaching and can hence only account for ~20% of the disappearance of $WH^{\bullet+}$.

25
26 ET from Y_{373} is hence the most plausible major cause of disappearance of $WH^{\bullet+}$ within a few
27 nanoseconds. For energetic reasons outlined in the Introduction, this ET step is likely to be coupled to
28 deprotonation of Y_{373} (PCET) and should be accompanied by an absorption increase around 405 nm due
29 to formation of a Y^{\bullet} radical (see solution spectrum in Figure 1B) that is superimposed to the strong
30 absorption increase due to the preceding formation of $FAD^{\bullet-}$ (Figure 1B). The WT signal at 405 nm (black
31 trace in Figure 4A) shows a minor (10-15%) absorption increase with kinetics consistent with the slower
32 phase (5.6 ns) of disappearance of $WH^{\bullet+}$ observed at $\lambda > 500$ nm. Within the first 1 ns after excitation,
33 there was, however, a slight absorption decrease at 405 nm. This is likely to be the result of an
34 overcompensation of a rise by partial decay of the strong absorption of $FAD^{\bullet-}$ due to its recombination
35 with $WH^{\bullet+}$ (see Discussion).

1
2
3 Because of the likely involvement of tyrosine deprotonation, we followed the kinetics of $\text{WH}^{\bullet+}$ in WT
4 *CraCRY* also at other pH values. Figure S2C shows the corresponding 562 nm signals at pH 6.5, 7.5, 8.4
5 (the "standard" pH for all other experiments shown here) and 9.0. All signals exhibit essentially the same
6 decay kinetics and also the same amplitudes of the decay (see SI, Section S2.2 for further details).
7
8
9

10 3.2.2. Nanosecond to second timescale

11
12 To complete our observations on the ns to s timescale, we used a TAS setup with ~5 ns time resolution
13 (see Section 2.3), with excitation pulses tuned at 475 nm. Figure 5 compares transient absorption
14 kinetics in the WT protein and in the Y373F mutant at three representative monitoring wavelengths (see
15 Figures S2 and S3 for additional wavelengths). Note that absolute signal amplitudes are not directly
16 comparable to those of the sub-ns setup due to different excitation conditions and different protein
17 concentrations.
18
19
20
21

22 Upon flash excitation, the signals recorded for the WT *CraCRY* up to 70 μs (Figure 5A, 5B) exhibit
23 step-like absorption changes, containing a very small and unresolved fast kinetic phase in ≤ 10 ns (minor
24 growth at 405 nm, minor decay at 562 nm and essentially no visible change at 457 nm). All signals
25 remain essentially constant within the time frames of Figure 5A and 5B and decay only on a much longer
26 timescale (in ~50 ms, see inset of Figure 5B). The amplitudes of the 562 nm signals amount to mere
27 ~10% of the amplitudes of the 457 nm signals (in absolute values) in WT *CraCRY*, indicating that there
28 are virtually no tryptophan radicals (protonated or deprotonated) left when the initial fast kinetic steps
29 are over. The remaining small positive signal at 562 nm can be attributed to the red tail in the
30 absorption spectrum of the $\text{FAD}^{\bullet-}$ radical (Figure 1B).
31
32
33
34
35
36

37 In the case of the Y373F mutant (Figure 5 C and D), all signals exhibit a biphasic and complete decay
38 ($\tau_1 \sim 260$ ns, $\tau_2 \sim 10$ μs). At the beginning of the time window of Figure 5C, the amplitude of the signal at
39 562 nm amounts to ~60 % of the signal at 457 nm and even after the first 260 ns phase, this number still
40 remains as high as ~45 % (Figure 5 C and D). This indicates that tryptophan radicals are present until the
41 decay is completed (in ~70 μs). In most members of the PCSf that contain the canonical tryptophan
42 triad, the distal (3rd) $\text{WH}^{\bullet+}$ radical deprotonates in several hundreds of nanoseconds,^{33,42} in competition
43 with recombination with $\text{FAD}^{\bullet-}$.⁴² This also seems to be the case for the Y373F mutant of *CraCRY*: While
44 the 260 ns phase represents ~30% of the signal decay at 405 and 457 nm (essentially due to $\text{FAD}^{\bullet-}/\text{WH}^{\bullet+}$
45 recombination), it represents ~50% at 562 nm (and even more at higher wavelengths) where both
46 recombination and deprotonation of $\text{WH}^{\bullet+}$ contribute (Figs. 6A and S3). The intrinsic time constants
47 for $\text{WH}^{\bullet+}$ deprotonation and $\text{FAD}^{\bullet-}/\text{WH}^{\bullet+}$ recombination derived from these data are ~400 ns and ~850
48
49
50
51
52
53
54
55
56
57
58
59
60

ns, respectively. The formed $\text{FAD}^{\bullet-}/\text{W}^{\bullet}$ radical pair decays completely with a time constant of $\sim 10 \mu\text{s}$ (see Figure 5D and Figure S3C), most likely by back ET coupled to re-protonation of the tryptophan.⁷⁶

Similarly, in the WT, the much slower $\text{FAD}^{\bullet-}/\text{Y}_{373}^{\bullet}$ recombination presumably proceeds via back ET and re-protonation of the tyrosine. It is of note that, at lower pH, a non-negligible fraction of $\text{FAD}^{\bullet-}$ gets protonated (in competition with back ET), creating a much longer-lived $\text{FADH}^{\bullet}/\text{Y}_{373}^{\bullet}$ pair (see Figure S2D and SI Section S2.2). The visible starting decay at the end of the blue trace in Figure S2D indicates that the lifetime of the $\text{FADH}/\text{Y}_{373}^{\bullet}$ pair is in the order of several seconds at pH 6.5.

4. DISCUSSION

Our experimental results are discussed below in chronological order of the photoinduced events during the light activation of *CraCRY*, focusing, however, on kinetics and mechanism of fast and efficient tyrosine oxidation that has no precedent in other members of the PCSf and is highly relevant for the understanding of proton coupled electron transfer (Section 4.2). A tentative reaction scheme is provided to facilitate the discussion (Scheme 1).

4.1. Reactions preceding tyrosine oxidation

4.1.1. Nature and kinetics of the photoproducts

Starting with the simpler case of Y373F, we find that the isotropic EADS (Figure 2C) are reminiscent of those previously reported for other members of the PCSf^{31,39,40} and, more specifically, highly similar to those of the W370F mutant of the 6-4 photolyase from *Xenopus laevis* (Xl64).³¹ In the latter mutant, the aromatic tetrad serving as ET chain in the WT is analogously reduced to the classical tryptophan triad, as in the Y373F mutant of *CraCRY*. Accordingly, EADS1 can be straightforwardly assigned to FAD_{ox}^* and EADS2 to the $\text{FAD}^{\bullet-}/\text{WH}^{\bullet+}$ radical pair formed by photoinduced ET from the proximal tryptophan (W_{399} in *CraCRY*) to FAD_{ox}^* in 0.43 ps. EADS3-5 reflect $\text{FAD}^{\bullet-}/\text{WH}^{\bullet+}$ states, in which the oxidation hole has migrated along the tryptophan triad (in competition with charge recombination), or relaxed states. In the present case, the initial photoreduction of the flavin produces a particular spectrum (EADS2), characterized by a very flat profile between *ca.* 500 and 620 nm. This shape becomes rounder in the EADS2→EADS3 transition (3.4 ps), and a clearer shallow maximum builds up around 600 nm, as expected for a $\text{WH}^{\bullet+}$ radical.⁷⁸ As mentioned in the case of Xl64,³¹ and following a hypothesis proposed by Immeln *et al.* for a plant cryptochrome,⁴¹ this evolution might be attributed to the cooling of $\text{WH}^{\bullet+}$ in a few ps, assuming this radical is initially produced in a hot state by the very fast primary photoreduction

1
2
3 of FAD_{ox} . Alternatively, one might attribute the unique shape of EADS2 to the proximal tryptophanyl
4 radical ($\text{W}_{399}\text{H}^{\bullet+}$), which would supposedly have a distinct absorption spectrum because of its specific
5 environment, *i.e.* deeply buried inside the protein and in close Coulombic interaction with the anionic
6 semiquinone radical ($\text{FAD}^{\bullet-}$). According to this hypothesis, the change of shape between EADS2 and
7 EADS3 would have to be assigned to a migration of the oxidation hole ($\text{WH}^{\bullet+}$) along the ET chain. The
8 transitions EADS3→EADS4 (41 ps) and EADS4→EADS5 (630 ps) represent only very weak absorption
9 changes in the Y373F mutant.

10
11 In the case of WT, the main difference with respect to the Y373F mutant is the final step (710 ps),
12 which leads to a strongly decreased absorption in the red part of the spectrum (see normalized EADS5 in
13 Figure 3). We have assigned this step to proton-coupled ET from Y_{373} to the terminal tryptophanyl cation
14 radical $\text{W}_{322}\text{H}^{\bullet+}$, yielding a long-lived $\text{FAD}^{\bullet-}/\text{Y}^{\bullet}$ radical pair (see Section 4.2). We recall that spectral
15 changes not seen in Y373F already arise during the 55-ps phase of WT (see Figure 3 and Figure S9). This
16 observation will be discussed below.

17
18 In order to establish more firmly the nature of EADS2 and EADS3, we fitted those spectra with a linear
19 combination of reference spectra of $\text{FAD}^{\bullet-}$ and $\text{WH}^{\bullet+}$, suitably scaled and shifted (see Section 2.2.2 and
20 Equation S4 in SI, Section S5.2), and complemented by the negative FAD_{ox} bleaching contribution. The
21 modification imposed on the $\text{FAD}^{\bullet-}$ reference spectrum (Figure S13, SI, Section S5.2) is relatively small,
22 while the $\text{WH}^{\bullet+}$ spectrum needs to be markedly shifted to the red (~20 nm). Such a shift, likely due to
23 the local environment of the tryptophanyl radical inside the protein, has been reported before also for
24 other PCSf proteins.^{31,40} The fits shown in Figure S12 are not perfect because the simple alterations
25 imposed on the reference spectra cannot completely reproduce the actual $\text{FAD}^{\bullet-}$ and $\text{WH}^{\bullet+}$ spectra
26 inside *CraCRY*. They nevertheless sufficiently support the hypothesis that EADS2 and EADS3 result from
27 the photoinduced reduction of FAD_{ox} by a tryptophan.

28
29 One may finally note for both WT and Y373F that the blue absorption and bleaching bands of EADS2
30 and EADS3 can be nearly superimposed (Figure 2). This suggests that almost no charge recombination of
31 the $\text{FAD}^{\bullet-}/\text{WH}^{\bullet+}$ pair, expected to induce a loss of transient absorption intensity, takes place during the
32 second kinetic phase. The main variation occurs in the red part of the spectrum, which was above
33 suggested to derive either from a cooling of the initial $\text{WH}^{\bullet+}$ radical or from the migration of the
34 oxidation hole to a different tryptophan.

35
36 As previously mentioned, the spectral evolution from EADS3 to EADS4 in WT is nearly absent in
37 Y373F (see Figure 3). Since a significant decay of the relative amplitude is observed around 600 nm, the
38 hypothesis of tyrosine oxidation during the 55-ps step has been considered but finally set aside for lack
39

of convincing evidence (see Section 4.2.1 and SI, Section S5.4). Alternatively, the EADS3→EADS4 spectral evolution of WT could be interpreted in terms of migration of the oxidation hole to W₃₂₂ and the building of a W₃₂₂H^{•+} population characterized by a specific (weaker) absorption in the presence of Y₃₇₃ (see SI, Section S5.4). As mentioned above, the 55-ps step is accompanied by partial charge recombination. According to the analysis in SI, Section 5.4, the corresponding yield is 23% (for this step only). However, given that the population losses during the preceding steps are probably small (extremely fast step one and almost no evolution of the bleaching band during step two), this number is likely close to the net yield of charge recombination counted from the initially excited flavin.

4.1.2. Migration of the oxidation hole along the Trp triad

In this section, we intend to use the anisotropy data to assign the WH^{•+} spectroscopic signatures detected in the transient absorption spectra to specific residues. Following an approach previously described in Refs.^{31,40}, we chose to probe WH^{•+} around 610 nm, expecting under these conditions that essentially a single transition of WH^{•+} is observed. Table 2 gathers the corresponding values of the EAAS (noted r_i), after initial decay of the excited state (averaged over 5 nm). Within experimental errors (of the order of ± 0.01), the r_i 's of WT and Y373F are rather similar, with a slightly larger difference for r_4 .

At this point, it is interesting to compare the experimental anisotropies to predictions based on the crystal structure of WT-CraCRY (PDB entry 5ZM0)⁷⁰ and on known directions of the transition dipole moments of FAD_{ox} and WH^{•+}, as previously described.^{31,40} Table 3 (line *raw*) gathers the anisotropies expected for each WH^{•+} radical of the ET chain if one could probe them independently.

These predictions may however not be fully comparable to the experimental anisotropies because a small contribution of FAD^{•-} could be present at 610 nm, as suggested by the fact that EADS5 keeps a positive value in this region in spite of the decay of WH^{•+}. Such a red tail of the FAD^{•-} spectrum has been reported before.^{79,80} From EAAS5 of WT in D₂O (less noisy than in H₂O), and neglecting the small amount of W₃₂₂H^{•+} reduced in 5 ns, the anisotropy of FAD^{•-} at 610 nm is estimated to be of the order of -0.1. If both WH^{•+} and FAD^{•-} contribute to the experimental anisotropy, the latter should be decomposed as follows:⁷¹

$$r_{\text{exp}} = x r_W + (1 - x) r_F \quad (\text{Eq. 3})$$

where r_W and r_F are the pure anisotropies respectively attached to WH^{•+} and FAD^{•-} and x is the relative contribution of WH^{•+} to the total isotropic signal. Taking $x = 0.8$ as a crude lower limit (a value of around 0.83 may be obtained from the modified WH^{•+} and FAD^{•-} of Figure S9), one gets new values listed in Table 3 (line *correction*), which provide a qualitative idea of the effect of the FAD^{•-} contribution on the predictions.

1
2
3 It first appears that r_2 is relatively close (within errors) to the predicted anisotropy of $W_{399}H^{\bullet+}$ that is
4 expected to be produced after primary reduction of the flavin by the proximal W_{399} residue. The possible
5 involvement of W_{401} in the first kinetic step is very unlikely since it is placed at a much larger distance of
6 FAD (7.9 Å; Figure 1A) than W_{399} (4.0 Å). In *EcCPDI* where the equivalent tryptophan (W_{384}) is only at
7 6.3 Å from FAD, Liu *et al.* found that the ET from W_{384} to FAD_{ox}^* takes place at a rate of $(80 \text{ ps})^{-1}$ in a
8 mutant lacking the proximal tryptophan.³⁷ An even slower rate is to be expected in *CraCRY*.
9

10
11 During the next step, the anisotropy changes sign and r_3 becomes positive as expected for $W_{376}H^{\bullet+}$,
12 the medial aromatic residue of the canonical tryptophan triad, however, without reaching its predicted
13 value. Since W_{332} is situated at a very close distance from W_{399} (3.8 Å; Figure 1A), it is possible that W_{332}
14 effectively competes with W_{376} for the reduction of $W_{399}H^{\bullet+}$, as previously reported for *EcCPDI* by Li *et*
15 *al.*³⁷ The resulting $W_{332}H^{\bullet+}$, expected to have a slightly less positive anisotropy than $W_{376}H^{\bullet+}$ (Table 3), is
16 then thought to contribute to the observed r_3 . In addition, the driving force of ET from W_{376} to $W_{399}H^{\bullet+}$
17 may be small, as claimed by Li *et al.*,³⁷ for the equivalent residues in *EcCPDI*, so that r_3 might be
18 diminished by a negative contribution from $W_{399}H^{\bullet+}$ still present at the end of the second ET step.
19 Finally, one may also hypothesize that r_3 takes a negative contribution from the distal $W_{322}H^{\bullet+}$, meaning
20 that delocalization of the oxidation hole has already reached the last tryptophan of the triad at this step
21 of the reaction. In any case, it appears that the oxidation hole is never wholly localized on W_{376} .
22
23

24
25 The values of r_4 and r_5 are more readily understood in the case of Y373F. We see that r_4 is quite close
26 to the expectation for $W_{322}H^{\bullet+}$, and that the match becomes even better for r_5 . This suggests that the
27 third kinetic step (41 ps in Y373F) results in a dominant localization of the oxidation hole on the W_{322}
28 site. The last step (630 ps) could either sign the final localization of the oxidation hole on W_{322} , if it were
29 not already completed and/or a rearrangement of the protein that stabilizes the $FAD^{\bullet-}/W_{322}H^{\bullet+}$ pair
30 (possibly required for a complete localization of the oxidation hole on W_{322}) and eventually blocks the
31 weak charge recombination channel still observed during this step. In the case of WT, the fourth and
32 possibly third kinetic steps are marked by the oxidation of the Y_{373} residue. Since Y^{\bullet} does not contribute
33 at 610 nm, Equation 3 would still apply but the x ratio would be smaller than in the absence of Y^{\bullet} . In the
34 limiting case of r_5 , one may assume that the amount of $WH^{\bullet+}$ is relatively small and take $x = 0$ as a rough
35 approximation. This leads to the estimation of r_f mentioned above (-0.1; from WT in D_2O). The case of r_4
36 is interesting because Equation 3 would predict a value situated somewhere between *ca.* -0.06 and -0.1
37 (depending on x) provided the oxidized tryptophan is W_{322} (see Table 3, line *raw*). The fact that r_4 has a
38 less negative value than that (Table 2; WT) suggests that the localization of the oxidation hole on W_{322} is
39
40
41
42
43
44
45
46
47
48
49
50
51
52
53
54
55
56
57
58
59
60

1
2
3 not finished at that step, and that other oxidized tryptophans contribute to this value, in particular
4 $W_{376}H^{\bullet+}$ because of its positive expected anisotropy. This consequently means that oxidation of Y_{373}
5 begins while there is still a certain degree of delocalization over different tryptophans. It might
6 reciprocally be speculated that the replacement of tyrosine by phenylalanine somehow enhances
7 protein and water reorganization leading to full localization of the oxidation hole on W_{322} during the
8 third kinetic step, as observed for Y373F.
9
10
11
12

13 14 **4.2. Oxidation of tyrosine Y_{373}**

15 *4.2.1. Kinetics and spectral changes*

16
17
18 In our attempts to establish the kinetics and the mechanism of oxidation of tyrosine Y_{373} in *CraCRY*, we
19 focused on kinetic and spectral features that depended on the presence of this tyrosine residue, *i.e.*
20 were absent or strongly modified in the Y373F mutant.
21
22

23 Our results obtained by both pump-probe and real-time TAS agree that reduction of a tryptophan
24 cation radical $WH^{\bullet+}$ occurs essentially with a time constant of ~ 600 - 700 ps in WT *CraCRY* (see Figures 3A,
25 5A and S2 (A-C)), while the same $WH^{\bullet+}$ species lives for ~ 250 nanoseconds in the Y373F mutant (Figures
26 6 (C,D) and S3). About 20% of this reduction is due to recombination with $FAD^{\bullet-}$ (observed as a partial
27 recovery of the FAD_{ox} bleaching band of around 450 nm; see Figures 3A and 5A) and about 80% should
28 hence be due to electron transfer from Y_{373} . Real-time TAS detected in addition a minor slower $WH^{\bullet+}$
29 reduction phase with a time constant of ~ 5 ns and approx. one third of the amplitude of the ~ 600 - 700 ps
30 phase. Neither variation of the pH (between 6.5 and 9.0; Figure S2C) nor use of a deuterated buffer
31 solution (Figure S8) had a significant effect on the reduction kinetics of $WH^{\bullet+}$.
32
33
34
35
36
37

38 Looking for a direct evidence of ultrafast tyrosine oxidation, we used the spectrally-resolved ultrafast
39 TAS data and focused on the fourth time component, fitted by a lifetime of 710 ps (transition from
40 EADS4 to EADS5). In order to characterize the spectral changes due to the reactive fraction of the
41 transient population, *i.e.* excluding charge recombination, EADS5 was fitted with a weighted sum of
42 EADS4, $WH^{\bullet+}$ and Y^{\bullet} contributions, as detailed in SI, Section S5.3 (Equation S5). The result shown in
43 Figure 6B (in $EADS5 - \phi EADS4$ form, where $1 - \phi$ is the yield of charge recombination occurring during
44 the $EADS4 \rightarrow EADS5$ step) provides a convincing support that $WH^{\bullet+}$ indeed undergoes reduction by a
45 tyrosine. The optimized parameters are available in SI, Section S5.3 (Table S2) and the modified
46 reference spectra are presented in Figure 6C. The $WH^{\bullet+}$ and Y^{\bullet} spectra providing the best fit of our
47 experimental data are found to be both red-shifted relative to solution spectra, by ~ 25 and 8 nm,
48 respectively (Figure 6C). It is worth noting that a 9-nm red shift of the Y^{\bullet} spectrum, as compared to a
49
50
51
52
53
54
55
56
57
58
59
60

1
2
3 reference spectrum in water, was also reported by Oldemeyer *et al.* in their time-resolved spectroscopic
4 study.²⁴ The fit also indicates that FAD^{•-}/WH^{•+} recombination (competing with the oxidation of Y₃₇₃)
5 occurs with a yield of 22%. We similarly attempted to fit EADS4 according to Equation S5 to check the
6 hypothesis of early oxidation of Y₃₇₃ (see Section 4.1.1). This approach however led to a conflicting
7 result, a large blue shift of the modified Y[•] spectrum, and was not considered conclusive (see more
8 details in SI, Section S5.4).
9

10 The kinetics of tyrosine oxidation should show up in our sub-ns/ns real time TAS data at 405 nm
11 (within the absorption band of Y[•]). The absorption rise due to the formation of Y[•] may, however, be
12 compensated of even overcompensated by the partial recombination of FAD^{•-}/WH^{•+} that is
13 accompanied by an absorption decrease at 405 nm (see spectra in Figure 1B). Such a compensation is
14 apparent in the ultrafast TAS data: while the uncorrected amplitudes around 400 nm slightly decrease
15 from 10 ps to 3.2 ns, (Figure S4 (B,C) and Figure S7), there is an increase after correction for
16 recombination of FAD^{•-}/WH^{•+} (compare NEADS3, 4 and 5 in Figure 3A). Similarly, no rise with $\tau \approx 600$ ps
17 was observed by real-time TAS at 405 nm (black trace in Figure 4A). A minor rise with $\tau \approx 5$ ns, in line
18 with the slower phase of WH^{•+} reduction, is however visible.
19

20 In an attempt to reconstruct the kinetics of tyrosine oxidation from the real-time TAS trace at 405 nm
21 by correcting for the FAD^{•-} contribution, we assumed that essentially only FAD_{ox}, FAD^{•-} and Y[•]
22 contribute at 405 nm (neglecting the weak contribution from WH^{•+}; see Figure 1B) and that the kinetics
23 of FAD^{•-} population is represented by the kinetics of the bleaching at 457 nm (blue trace in Figure 4A;
24 here we also neglect a weak contribution from WH^{•+}). Subtraction of the 457 nm trace (inverted and
25 rescaled to the same initial amplitude) from the 405 nm trace yielded a "corrected" 405 nm signal
26 (Figure 6A) that we consider to be a coarse approximation of the kinetics of tyrosine oxidation (see SI,
27 Section S2.1 for more details on how the corrected 405 nm signal was constructed). A biexponential fit
28 of the corrected signal (using Equation S2) yielded time constants of 820 ps (with an amplitude of ~6
29 mOD) and 6.0 ns (with an amplitude of ~3 mOD). The tyrosine oxidation hence follows essentially the
30 same biphasic kinetics as WH^{•+} reduction (~600-700 ps and ~5 ns) observed above 500 nm, confirming
31 that Y₃₇₃ is oxidized by a tryptophanyl cation radical, most likely the distal W₃₂₂H^{•+}.
32
33
34
35
36
37
38
39
40
41
42
43
44
45
46
47

48 Let us finally emphasize that, according to our spectral analysis (Figure 6B), the oxidized tyrosine is
49 observed in its deprotonated Y[•] form. The protonated YH^{•+} radical cation has recently been reported in
50 a flavoenzyme to have a strongly displaced spectrum around 490 nm⁸¹, which would not match our
51 observations (see also the lack of induced absorption at 488 nm in the real-time TAS data; green trace in
52 Figure 4A). Tyrosyl deprotonation is thus intimately involved in the process that must be considered a
53
54
55
56
57
58
59
60

case of proton-coupled electron transfer (PCET).⁶⁴ It should be noted that, according to the above analyses, the observed 600-700 ps time constant results from a competition between reduction of $\text{WH}^{\bullet+}$ by PCET from Y_{373} and approximately four times slower recombination with $\text{FAD}^{\bullet-}$. The intrinsic rate constant of the major phase of PCET would thus be of the order of $(800\text{-}900\text{ ps})^{-1}$. We will adopt an approximate value of $(800\text{ ps})^{-1}$ for the discussion of the PCET mechanism presented in the following section.

4.2.2. Reaction mechanism of tyrosine oxidation

As discussed above, the reduction of $\text{WH}^{\bullet+}$ by PCET from Y_{373} in *CraCRY* mostly proceeds with an intrinsic rate constant of $(800\text{ ps})^{-1}$. This is substantially faster than the fastest phase of oxidation of the so-called tyrosine-Z in oxygen-evolving PSII ($\tau \sim 30\text{ ns}$). Remarkably, in both cases the reaction kinetics was found to be independent of pH (between 6.5 and 9.0 in *CraCRY* (Figure S2C) and between 4.5 and 7.5 in PSII⁸²) and was not significantly affected by deuteration of the buffer solution (Table 1).⁸³⁻⁸⁵

The structure of *CraCRY* (Figure 1A) strongly suggests that the electron acceptor is $\text{W}_{322}\text{H}^{\bullet+}$, the distal member of the canonical Trp triad, because it is located at only 3.8 Å edge-to-edge distance from Y_{373} . The proton acceptor is likely to be aspartate D_{321} that forms a hydrogen bond with the Y_{373} hydroxyl group (3.0 Å; Figure 1A).⁷⁰

In the following, we discuss possible reaction mechanisms in the framework of limiting cases of PCET following the classification by Hammes-Schiffer and Stuchebrukhov⁶⁴ and Liu *et al.*⁸⁶ The reaction pathways considered for *CraCRY* and our notations are shown in Scheme 1. We note that based on published reduction potentials and pK_a values in aqueous solution of the amino acid side chains involved, namely $E^\circ(\text{WH}^{\bullet+}/\text{WH}) \approx 1.07\text{ V}$ vs. NHE,⁵⁴ $E^\circ(\text{YH}^{\bullet+}/\text{YH}) \approx 1.35\text{ V}$,⁵⁴ $E^\circ(\text{Y}^\bullet/\text{Y}^-) \approx 0.65\text{ V}$,⁵⁴ $\text{pK}_a(\text{YH}^{\bullet+}/\text{Y}^\bullet) \approx -2$,⁶⁰ $\text{pK}_a(\text{YH}/\text{Y}^-) \approx 9.9$,⁵⁴ and $\text{pK}_a(\text{DH}/\text{D}^-) = 3.9$,⁸⁷ the overall PCET reaction would be downhill by 0.07 eV. ET as the first step would, however, be uphill by 0.28 eV and PT as the first step even by 0.35 eV. As discussed below, these values may be modified considerably by the protein environment and by interactions between the species.

(I) Sequential ET/PT (blue pathway in Scheme 1)

(Ia) PT is "fast" ($k_{\text{PT}} \gg k_{\text{BET}}$)

PT takes immediately place when the "activated" state $[\text{W}_{322}\text{H} \text{Y}_{373}\text{H}^{\bullet+} \cdots \text{D}_{321}^-]$ is reached by uphill ET. The uphill ET is hence rate limiting.

$$k_{\text{PCET}} = k_{\text{FET}}$$

(Ib) PT is "slow" ($k_{\text{PT}} \ll k_{\text{BET}}$)

Several ET "attempts" are needed to complete the reaction by PT. In other words, PT occurs from an ET pre-equilibrium in which the "activated" state $[W_{322}H Y_{373}H^{\bullet+} \cdots D_{321}^-]$ has low population.

$$k_{PCET} = k_{PT} K_{ET} \text{ with } K_{ET} = k_{FET}/k_{BET} = \exp(-\Delta G^{\circ}_{ET}/k_B T)$$

(II) Sequential PT/ET (red pathway in Scheme 1)

(IIa) ET is "fast" ($k_{ET} \gg k_{BPT}$)

The ET takes place immediately when the "activated" state $[W_{322}H^{\bullet+} Y_{373}^- \cdots HD_{321}]$ is reached by the uphill PT. The uphill PT is hence rate limiting.

$$k_{PCET} = k_{FPT}$$

(IIb) ET is "slow" ($k_{ET} \ll k_{BPT}$)

Several PT "attempts" are needed to complete the reaction by the ET. In other words, the ET occurs from a PT pre-equilibrium in which the "activated" state $[W_{322}H^{\bullet+} Y_{373}^- \cdots HD_{321}]$ has low population.

$$k_{PCET} = k_{ET} K_{PT} \text{ with } K_{PT} = k_{FPT}/k_{BPT} = \exp(-\Delta G^{\circ}_{PT}/k_B T)$$

(III) Concerted PCET (green pathway in Scheme 1)

ET and PT occur together in one step, avoiding formation of a high energy intermediate.

No simple rate equation can be given.

Among these cases, Ib and IIa are expected to show a significant normal H/D KIE because the rate of forward PT enters directly into the rate equation. For concerted PCET (case III), a substantial normal KIE is considered to be a hallmark.^{64††} Because of the absence of a significant KIE for $W_{322}H^{\bullet+}$ reduction by Y_{373} in *CraCRY*, we focus on the two remaining cases.

For *sequential ET/PT with "fast" PT* (case Ia), the overall rate is given by the (uphill) forward ET. The expected rate of this ET step at room temperature may be estimated using the following semi-empirical expression for the rate k_{ET}^{en} (in s^{-1}) of endergonic ET in proteins at room temperature:⁸⁹

$$\log k_{ET}^{en} = 13.0 - (1.2 - 0.8\rho)(R - 3.6) - 3.1(-\Delta G^{\circ} + \lambda)^2/\lambda - \Delta G^{\circ}/0.06 \quad (\text{Eq. 4})$$

where R is the edge-to-edge distance between electron donor and acceptor (in Å), ΔG° the (positive) standard Gibbs free energy (in eV) of the ET and λ the reorganization energy (in eV). ρ represents the packing density of protein atoms in the volume between electron donor and acceptor.

†† A recent theoretical work⁸⁸ presented special cases with negligible KIE, in which highly excited (several eV) electron-proton vibronic states dictated the dynamics. Such highly excited states are not expected to play a role in PCET between tyrosine and tryptophan in *CraCRY*.

Using $R = 3.8 \text{ \AA}$ (Figure 1A), $\Delta G^\circ = 0.28 \text{ eV}$ (see above), $\lambda = 1 \text{ eV}$ (considered as “unremarkable” in Ref.⁸⁹ and $\rho = 0.76$, an average value for ET reactions in proteins,⁸⁹ Equation 4 yields $k_{\text{ET}}^{\text{en}} = (250 \text{ ns})^{-1}$, *i.e.* more than two orders of magnitude slower than the rate of $\sim(800 \text{ ps})^{-1}$ as deduced from the observed kinetics (see above). The somewhat arbitrarily chosen value of ρ is not critical in this evaluation because the term $(R - 3.6)$ is small. The also not well known λ has more impact, but even when choosing the optimal value $\lambda = \Delta G^\circ$, the calculated rate of $(6.1 \text{ ns})^{-1}$ is still slower by an order of magnitude than the observed rate. Most critical in this evaluation is the endergonic degree of the reaction. Keeping $\lambda = 1 \text{ eV}$, a value of $\Delta G^\circ = 0.0642 \text{ eV}$ would be required to get a rate of $(800 \text{ ps})^{-1}$, *i.e.* far below the value of 0.28 eV estimated above. We however do not exclude that the protein environment and the interactions between the species may have such a strong effect on the energetics, for the following reasons:

- (1) The reduction potential of $\text{WH}^{\bullet+}/\text{WH}$ embedded in the protein matrix is expected to be higher than in aqueous solution (1.07 V) because the positive charge is less stabilized in a low dielectric environment. *E.g.*, the reduction potentials of members of the canonical Trp triad in oxidized *EcCPDI* were estimated to $\geq 1.48, 1.41$ and 1.24 V vs NHE ³⁷ in the order of increasing distance from FAD, similar to estimations that can be deduced from the energetics in semi-reduced *EcCPDI*.³⁶ The large drop from the medial to the distal Trp in *EcCPDI* can be understood as a stabilization of the positive charge by the proximity of the aqueous phase^{36,37} and may be less pronounced in *CraCRY* because of the presence of Y_{373} .^{**}
- (2) The negative charge of aspartate D_{321}^- in close proximity of Y_{373} may decrease the $\text{YH}^{\bullet+}/\text{YH}$ reduction potential due to electrostatic stabilization of the positive charge.

Case Ia further requires that the subsequent PT is much faster than back ET ($k_{\text{PT}} \gg k_{\text{BET}}$). Back ET would be exergonic and its rate may be estimated by Equation 5.⁸⁹

$$\log k_{\text{ET}}^{\text{ex}} = 13.0 - (1.2 - 0.8\rho)(R - 3.6) - 3.1(\Delta G^\circ + \lambda)^2/\lambda \quad (\text{Eq. 5})$$

Using $\Delta G^\circ = -0.0642 \text{ eV}$, $\lambda = 1 \text{ eV}$ and the other parameters as above, one obtains $k_{\text{BET}} = k_{\text{ET}}^{\text{ex}} = (68 \text{ ps})^{-1}$.

Based on the solution $\text{p}K_{\text{a}}$ values given above, PT from $\text{Y}_{373}\text{H}^{\bullet+}$ to D_{321}^- would be downhill by 0.35 eV . The PT distance would be at least 1.0 \AA based on the 3.0 \AA hydrogen bond length in the crystal structure (Figure 1A) and assuming an O-H distance of 1.0 \AA both in the reactant $\text{Y}_{373}\text{H}^{\bullet+}$ and in the product D_{321}H . Proton transfer in hydrogen bonds can be as fast as tens of femtoseconds over a distance of approx.

** Our data by ultra-fast spectroscopy indicate that $\text{W}_{322}\text{H}^{\bullet+}$ is less stabilized in the WT than in the Y373F mutant; see Section 4.1.2.

1
2
3 0.6 Å in the excited state of 1-hydroxy-2-acetonaphthone⁹⁰ or at most a few picoseconds over approx.
4 0.7 Å (O-H...O hydrogen bond length of 2.7 Å) in green fluorescent protein^{91,92} but depends very
5 strongly on the transfer distance, decreasing typically by one order of magnitude per 0.07 Å.⁹³ It is hence
6 questionable that proton transfer from $Y_{373}H^{*+}$ to D_{321}^- can be faster than back ET from W_{322} to $Y_{373}H^{*+}$.
7
8 We note, however, that formation of $Y_{373}H^{*+}$ may induce structural changes (*e.g.* due to electrostatic
9 interaction with D_{321}^-) that decrease the proton transfer distance relative to the (dark state) crystal
10 structure.
11
12
13
14

15 For *sequential PT/ET with "slow" ET* (case IIb), the overall rate is determined by the product of the PT
16 (pre-)equilibrium constant K_{PT} and the rate constant k_{ET} of the subsequent ET. There should be no
17 significant KIE,⁶⁴ because the effects on the forward and backward PT are usually similar and cancel each
18 other out in the rate expression.⁵⁵
19
20
21

22 Based on the solution values given above, PT from $Y_{373}H$ to D_{321}^- would be uphill by $\Delta G^{\circ}_{PT(1)} = 0.35$ eV
23 and $K_{PT} = 10^{-6}$. Subsequent ET from Y_{373}^- to $W_{322}H^{*+}$ would be downhill by 0.42 eV, yielding an ET rate of
24 $(1.5 \text{ ps})^{-1}$ according to Equation 5 with the other parameters as above, and an overall rate of $(1.5 \mu\text{s})^{-1}$.
25 Assuming the optimal reorganization energy $\lambda = -\Delta G^{\circ} = 0.42$ eV, the ET rate would be $(130 \text{ fs})^{-1}$ and the
26 overall rate $(130 \text{ ns})^{-1}$, still very far off the experimental rate of $(800 \text{ ps})^{-1}$. To obtain the rate of
27 $(800 \text{ ps})^{-1}$, the PT (pre-)equilibrium constant would have to be $> 1.6 \times 10^{-4}$, corresponding to $\Delta G^{\circ}_{PT} < 0.22$
28 eV and a pK_a difference < 3.8 (as compared to 6.0 according to solution values; see above). We would
29 not exclude such a strong modification of the PT equilibrium, because:
30
31
32
33
34

- 35 (1) pK_a values of amino acid side chains in proteins can deviate substantially from solution values.⁸⁷
36
37 (2) The presence of $W_{322}H^{*+}$ close to Y_{373} is likely to stabilize Y_{373}^- by electrostatic interaction and
38 hence to decrease the endergonicity of PT from Y_{373} to D_{321}^- .
39

40 Case IIb further requires that (downhill) back PT is much faster than ET ($k_{ET} \ll k_{BPT}$), *i.e.* well in the sub-
41 picosecond range. As discussed above for case Ia, it is questionable that such a fast proton transfer is
42 possible at the distance in the (dark-state) crystal structure. One should, however, not exclude the
43 possibility that formation of $W_{322}H^{*+}$ induces a shortening of the hydrogen bond between Y_{373} and D_{321} .
44
45
46

47 Our experimental data indicated that a minor fraction of Y_{373} was oxidized at a slower rate of
48 $\sim (5 \text{ ns})^{-1}$. This may reflect some conformational heterogeneity of *CraCRY* that affects ET or PT distances
49 or energetics, but may also be explained by an energetic relaxation of $W_{322}H^{*+}$ due to reorganization of
50
51

52
53 ⁵⁵ A remarkable exception was recently reported for PCET involving a metal hydride with an appended pyridine
54 base: a substantial inverse KIE was observed and attributed to an isotope effect on the PT (pre)equilibrium
55 constant due to differences in the zero point energy of the metal-H and H⁺-pyridine vibrations.⁸⁶
56
57
58
59
60

1
2
3 the protein environment that occur in competition with the oxidation of Y_{373} in 800 ps (large white
4 arrow in Scheme 1). Relaxed $W_{322}H^{*+}$ would have a lower reduction potential, and hence, for sequential
5 ET/PT (case Ia), ET would be more uphill and the overall reaction would slow down. In the sequential
6 PT/ET scenario (case IIb), ET would be less downhill and the overall reaction would slow down as well
7 (except if ET occurred in the Marcus inverted region (*i.e.* $-\Delta G^\circ > \lambda$), which is highly unlikely given the
8 moderate driving force). The free energy decrease due to relaxation would have to be in the order of
9 0.07 and 0.2 eV in cases Ia and IIb, respectively, to account for a slowdown of the overall reaction to ~ 5
10 ns.
11

12 We finally would like to compare tyrosine oxidation in *CraCRY* with oxidation of tyrosine-Z by $P680^{*+}$
13 in oxygen evolving PSII that has been studied experimentally for 40 years and is still the subject of
14 controversial discussions.⁴⁸⁻⁵³ The fastest kinetics in PSII has a time constant of ~ 30 ns⁵⁶⁻⁵⁸ and does not
15 show a significant KIE.⁸³⁻⁸⁵ The reduction potential of $P680^{*+}/P680$ is ~ 1.25 V,⁵⁵ *i.e.* 0.1 V below the
16 solution potential of YH^{*+}/YH , and probably even more below that of Y_zH^{*+}/Y_zH in a protein.⁵⁴ The edge-
17 to-edge distance between $P680$ and Y_z is 9.0 Å,⁵³ as compared to 3.8 Å between Y_{373} and D_{321} in *CraCRY*.
18 Y_z forms a strong H-bond with a histidine residue (O-N distance, 2.5 Å,⁹⁴ as compared to 3.0 Å for the
19 hydrogen bond between Y_{373} and D_{321} in *CraCRY*). As for tyrosine oxidation in *CraCRY*, the absence of a
20 significant KIE suggests either a sequential ET/PT with PT being "fast" (case Ia) or a sequential PT/ET with
21 ET being "slow" (case IIb)^{***}. Case Ia seems, however, to be excluded in PSII because the rate limiting
22 uphill ET from Y_z to $P680^{*+}$ is expected to take ≥ 500 ns according to Equation 4 using $\rho = 0.75$, $R = 9$ Å, λ
23 = 0.77 eV (all from Ref. ⁵³) and $\Delta G^\circ \geq 0.1$ eV. A recent analysis suggested sequential PT/ET with a PT (pre-
24 equilibrium constant of 0.16 and an ET rate of $(7.7 \text{ ns})^{-1}$.⁵³ QM/MM calculations on PSII indicate that the
25 two energy minima of the proton location are very shallow and only ~ 0.4 Å apart,¹⁰⁰ presumably
26 allowing ultrafast and nearly activationless PT.
27

28 For the even faster tyrosine oxidation in *CraCRY*, the substantially longer hydrogen bond between
29 Y_{373} and D_{321} in the dark state crystal structure does not support a sequential PT/ET mechanism unless
30 formation of $W_{322}H^{*+}$ substantially shortens this bond and shifts the PT (pre-)equilibrium towards Y_{373}^-
31 $\cdots HD_{321}$ (see above). The very short ET distance in *CraCRY*, however, could enable sequential ET/PT,
32
33
34
35
36
37
38
39
40
41

42
43
44
45
46
47
48
49
50
51
52 *** Concerted PCET has been suggested for tyrosine oxidation in PSII with inactivated oxygen evolution,⁴⁹ where the
53 environment of tyrosine-Z is substantially modified.^{51,53} In this case tyrosine oxidation by $P680^{*+}$ is slower and pH
54 dependent (time constants from ~ 300 ns at pH 9 to ~ 50 μ s at pH 4^{95,96} and shows a significant normal H/D KIE at
55 pH < 8.⁹⁷⁻⁹⁹
56
57
58
59
60

1
2
3 provided that the protein environment decreases the endergonic character of ET from $Y_{373}H$ to $W_{322}H^{*+}$
4 relative to the solution value (see above).
5

6 Tyrosine oxidation during photoactivation of the Slr 1694 BLUF domain of *Synechocystis PCC6803*
7 occurs by sequential ET (from Y_8 to the photoexcited FAD cofactor; edge-to-edge distance, 3.5 Å) and PT
8 (from Y_8H^{*+} to $FAD^{\bullet-}$ via Q_{50}) on a time scale of tens of picoseconds,⁶¹ *i.e.* two orders of magnitude faster
9 than tyrosine oxidation by $W_{322}H^{*+}$ in *CraCRY*. A main cause of the much faster kinetics is likely the much
10 more favorable energetics of ET in Slr 1694 BLUF, which was estimated to be downhill because of the
11 high energy of FAD_{ox}^* ,^{61,101,102} but uphill in the oxidation of Y_{373} in *CraCRY*. The term PCET has been used
12 for the overall process of tyrosine oxidation during photoactivation of Slr1694 BLUF,^{63,67} despite ET as
13 the first step of the sequential ET/PT being downhill (cf. Introduction). A very recent work named it
14 electron-coupled double proton transfer.¹⁰²
15
16
17
18
19
20
21
22
23

24 **4.3. Fate of the $FAD^{\bullet-}/Y_{373}^{\bullet}$ pair and efficiency of FAD photoreduction**

25
26 The light-induced ET and PT reactions leading to FAD reduction occur in competition with non-
27 productive recombination (see Scheme 1). The quantum yield of FAD reduction can be estimated from
28 the time course of the amplitude of the bleaching of the main absorption band of oxidized FAD around
29 450 nm. Our data by ultrafast TAS indicate that in WT *CraCRY* 40-45% of the initially formed $FAD^{\bullet-}$
30 (represented by EADS2 in Fig. 3A) is lost during formation of the $FAD^{\bullet-}/Y_{373}^{\bullet}$ pair (represented by EADS5
31 in Fig. 3A). No significant further losses were detected by real time TAS up to 70 μs (Fig. 6). The quantum
32 yield of the initial ET from W_{399} to excited FAD ($^1FAD_{ox}^*$) in ~ 0.4 ps is likely to be virtually 100% as this
33 process is several orders of magnitude faster than the lifetime of singlet excited flavins in the absence of
34 quenching by ET (a few ns¹⁰³). We conclude that the $FAD^{\bullet-}/Y_{373}^{\bullet}$ pair is formed with a quantum yield of
35 $\sim 60\%$.
36
37
38
39
40
41
42

43 The $FAD^{\bullet-}/Y_{373}^{\bullet}$ pair in isolated WT *CraCRY* at pH 8.4 finally decayed by recombination in tens of
44 milliseconds (Figure 5B, inset), in line with a previous report.²⁹ We found that this recombination is in
45 competition with protonation of $FAD^{\bullet-}$ to form the neutral, red light-absorbing radical $FADH^{\bullet}$ that is the
46 primary target for *CraCRY*-based red light responses of *Chlamydomonas* cells.^{21,22,104} The protonation
47 was accelerated and hence more efficient at lower pH (see Figure S2D and SI, Section S2.2 for more
48 details), explaining a previous observation²³ that the amplitude of blue light-induced very long-lived
49 bleaching of the FAD absorption band in the blue (attributed to formation of $FADH^{\bullet}$) increased strongly
50 with decreasing pH. One would expect that the $FADH^{\bullet}/Y_{373}^{\bullet}$ pair recombines via activated re-formation
51
52
53
54
55
56
57
58
59
60

1
2
3 of $\text{FAD}^{\bullet-}/\text{Y}_{373}^{\bullet}$ (the blue trace in Figure S2D (pH 6.5) was measured up to 600 ms and indicated an onset
4 of recombination with a time constant in the order of seconds) and that light-generated FADH^{\bullet} in
5 *CraCRY* can live for minutes only when its recombination partner Y_{373}^{\bullet} is quenched by reduction. Given
6 the unusually long lifetime of the $\text{FADH}^{\bullet}/\text{Y}_{373}^{\bullet}$ pair, it seems likely that even trace amounts of reducing
7 agents have enough time to act upon the Y_{373}^{\bullet} radical, leading to accumulation of metastable FADH^{\bullet} .
8 Remarkably, on a time scale up to a few nanoseconds, there are less losses by recombination in in the
9 Y373F mutant protein (~20%) than in WT (~40%; Figures 3A and 3C). This may indicate that the
10 $\text{FAD}^{\bullet-}/\text{W}_{322}\text{H}^{\bullet+}$ pair relaxes more rapidly and/or more deeply in the mutant (*cf.* end of Section 4.1.2),
11 increasing the barrier for recombination via reformation of the primary pair $\text{FAD}^{\bullet-}/\text{W}_{399}\text{H}^{\bullet+}$ (see Scheme
12 1). The presence of Y373 as fourth member of the ET chain in WT *CraCRY* appears, however, to be
13 required to obtain a long-lived radical pair as $\text{FAD}^{\bullet-}/\text{W}_{322}^{\bullet}$ in the Y373F mutant recombines in 10 μs as
14 compared to 50 ms for the $\text{FAD}^{\bullet-}/\text{Y}_{373}^{\bullet}$ pair in WT.
15
16
17
18
19
20
21
22
23
24
25
26

27 5. CONCLUDING REMARKS

28
29 The main result of the present study is our demonstration of a very fast photoinduced proton-coupled
30 electron transfer (PCET)⁶⁴ from tyrosine to tryptophan in WT-*CraCRY*, forming the neutral
31 (deprotonated) tyrosyl radical of Y_{373}^{\bullet} in ~800 ps without significant H/D KIE. This PCET step is about 40
32 times faster than formation of the tyrosyl radical Y_2^{\bullet} in oxygen evolving PSII. Our results may either be
33 explained by a sequential ET/PT with fast PT or a sequential PT/ET with slow ET (see detailed discussion
34 in Section 4.2.2). Quantum mechanical/molecular mechanical (QM/MM) calculations may provide
35 crucial information to decide which mechanism is actually preferred by *CraCRY* and how it is
36 implemented. In particular, it would be useful to estimate the rate of PT from $\text{Y}_{373}\text{H}^{\bullet+}$ to D_{321}^- in order to
37 evaluate whether sequential ET/PT as fast as 800 ps and not rate-limited by PT is possible. As far as the
38 validity of PT/ET is concerned, it would be interesting to determine if the formation of $\text{W}_{322}\text{H}^{\bullet+}$ could
39 induce any shortening of the hydrogen bond between Y_{373} and D_{321} , thereby allowing a very fast back PT
40 from D_{321}H to Y_{373}^- ($k_{\text{ET}} \ll k_{\text{BPT}}$; see Section 4.2.2), which in turn could ensure the lack of a KIE. Further
41 experimental developments should involve checking the identity of the proton acceptor by point
42 mutation of D_{321} to a non-H-acceptor residue and studies of the temperature dependence of the
43 tyrosine oxidation kinetics for estimating the barrier of the putative uphill step in sequential PCET.
44
45
46
47
48
49
50
51
52
53
54
55
56
57
58
59
60

1
2
3 It is finally worth recalling that CraCRY is uniquely characterized by its ability to function as a red light
4 receptor *in vivo* and to accumulate FADH• *in vitro* even in the (alleged) absence of external reductant.²⁰
5 Our results demonstrate that the FAD•⁻ Y₃₇₃• pair is formed with a high quantum yield (~60%) and has a
6 long intrinsic lifetime (~50 ms due to recombination). The semi-reduced FAD may therefore be easily
7 stabilized by protonation of FAD•⁻ (to form the red-absorbing FADH•) and by reduction of its partner
8 Y₃₇₃• by even trace amounts of residual reducing agents. All these factors are congruent with the unique
9 properties of CraCRY *in vivo*.
10
11
12
13
14
15
16
17

18 ACKNOWLEDGEMENTS

19
20 This work obtained financial support by the International Max Planck research school for Environmental,
21 Cellular and Molecular Biology (SF), the Deutsche Forschungsgemeinschaft (LOE: FOR 1261-2, ES 152/12-
22 1), the Air Force Office of Scientific Research (AFOSR; grant No FA9550-14-1-0409) and by the French
23 Infrastructure for Integrated Structural Biology (FRISBI: ANR-10-INBS-05).
24
25
26
27

28 REFERENCES

- 29
30 (1) Sancar, A. Structure and Function of DNA Photolyase and Cryptochrome Blue-Light
31 Photoreceptors. *Chem. Rev.* **2003**, *103*, 2203.
32 (2) Lin, C. T.; Shalitin, D. Cryptochrome Structure and Signal Transduction. *Annu. Rev. Plant Biol.* **2003**,
33 *54*, 469.
34 (3) Chaves, I.; Pokorny, R.; Byrdin, M.; Hoang, N.; Ritz, T.; Brettel, K.; Essen, L.-O.; van der Horst, G. T.
35 J.; Batschauer, A.; Ahmad, M. The Cryptochromes: Blue Light Photoreceptors in Plants and
36 Animals. *Annu. Rev. Plant Biol.* **2011**, *62*, 335.
37 (4) Hore, P. J.; Mouritsen, H. The Radical-Pair Mechanism of Magnetoreception. *Annu. Rev. Biophys.*
38 **2016**, *45*, 299.
39 (5) Cadet, J.; Sage, E.; Douki, T. Ultraviolet Radiation-Mediated Damage to Cellular DNA. *Mutation*
40 *Res.* **2005**, *571*, 3.
41 (6) Weber, S. Light-Driven Enzymatic Catalysis of DNA Repair: A Review of Recent Biophysical Studies
42 on Photolyase. *Biochim. Biophys. Acta Bioenerg.* **2005**, *1707*, 1.
43 (7) Brettel, K.; Byrdin, M. Reaction Mechanisms of DNA Photolyase. *Curr. Opin. Struct. Biol.* **2010**, *20*,
44 693.
45 (8) Zhong, D. Electron Transfer Mechanisms of DNA Repair by Photolyase. *Annu. Rev. Phys. Chem.*
46 **2015**, *66*, 691.
47 (9) Selby, C. P.; Sancar, A. A Cryptochrome/Photolyase Class of Enzymes with Single-Stranded DNA-
48 Specific Photolyase Activity. *Proc. Natl. Acad. Sci. USA* **2006**, *103*, 17696.
49 (10) Pokorny, R.; Klar, T.; Hennecke, U.; Carell, T.; Batschauer, A.; Essen, L. O. Recognition and Repair of
50 UV Lesions in Loop Structures of Duplex DNA by DASH-Type Cryptochrome. *Proc. Natl. Acad. Sci.*
51 *USA* **2008**, *105*, 21023.
52
53
54
55
56
57
58
59
60

- 1
2
3 (11) Berrocal-Tito, G. M.; Esquivel-Naranjo, E. U.; Horwitz, B. A.; Herrera-Estrella, A. Trichoderma
4 Atroviride PHR1, a Fungal Photolyase Responsible for DNA Repair, Autoregulates its Own
5 Photoinduction. *Eukaryotic Cell* **2007**, *6*, 1682.
- 6 (12) Bayram, O.; Biesemann, C.; Krappmann, S.; Galland, P.; Braus, G. H. More Than a Repair Enzyme:
7 *Aspergillus nidulans* Photolyase-Like CryA Is a Regulator of Sexual Development. *Molec. Biol. Cell*
8 **2008**, *19*, 3254.
- 9 (13) Coesel, S.; Mangogna, M.; Ishikawa, T.; Heijde, M.; Rogato, A.; Finazzi, G.; Todo, T.; Bowler, C.;
10 Falciatore, A. Diatom PtCPF1 Is a New Cryptochrome/Photolyase Family Member with DNA Repair
11 and Transcription Regulation Activity. *EMBO Rep.* **2009**, *10*, 655.
- 12 (14) Heijde, M.; Zabulon, G.; Corellou, F.; Ishikawa, T.; Brazard, J.; Usman, A.; Plaza, P.; Martin, M. M.;
13 Falciatore, A.; Todo, T.; Bouget, F.-Y.; Bowler, C. Characterization of Two Members of the
14 Cryptochrome / Photolyase Family from *Ostreococcus Tauri* Gives Insight in the Origin and
15 Evolution of Cryptochromes. *Plant Cell Environ.* **2010**, *33*, 1614.
- 16 (15) Kiontke, S.; Geisselbrecht, Y.; Pokorny, R.; Carell, T.; Batschauer, A.; Essen, L.-O. Crystal Structures
17 of an Archaeal Class II DNA Photolyase and its Complex with UV-Damaged Duplex DNA. *EMBO J.*
18 **2011**, *30*, 4437.
- 19 (16) Geisselbrecht, Y.; Fruehwirth, S.; Schroeder, C.; Pierik, A. J.; Klug, G.; Essen, L.-O. CryB from
20 *Rhodobacter Sphaeroides*: A Unique Class of Cryptochromes with New Cofactors. *EMBO Rep.*
21 **2012**, *13*, 223.
- 22 (17) Juhas, M.; von Zadow, A.; Spexard, M.; Schmidt, M.; Kottke, T.; Buechel, C. A Novel Cryptochrome
23 in the Diatom *Phaeodactylum tricornutum* Influences the Regulation of Light-Harvesting Protein
24 Levels. *FEBS J.* **2014**, *281*, 2299.
- 25 (18) Oliveri, P.; Fortunato, A. E.; Petrone, L.; Ishikawa-Fujiwara, T.; Kobayashi, Y.; Todo, T.; Antonova,
26 O.; Arboleda, E.; Zantke, J.; Tessmar-Raible, K.; Falciatore, A. The Cryptochrome/Photolyase Family
27 in Aquatic Organisms. *Mar. Genom.* **2014**, *14*, 23.
- 28 (19) Zhang, M.; Wang, L.; Zhong, D. Photolyase: Dynamics and Mechanisms of Repair of Sun-Induced
29 DNA Damage. *Photochem. Photobiol.* **2017**, *93*, 78.
- 30 (20) Beel, B.; Prager, K.; Spexard, M.; Sasso, S.; Weiss, D.; Mueller, N.; Heinnickel, M.; Dewez, D.;
31 Ikoma, D.; Grossman, A. R.; Kottke, T.; Mittag, M. A Flavin Binding Cryptochrome Photoreceptor
32 Responds to Both Blue and Red Light in *Chlamydomonas Reinhardtii*. *Plant Cell* **2012**, *24*, 2992.
- 33 (21) Kottke, T.; Oldemeyer, S.; Wenzel, S.; Zou, Y.; Mittag, M. Cryptochrome Photoreceptors in Green
34 Algae: Unexpected Versatility of Mechanisms and Functions. *J. Plant Physiol.* **2017**, *217*, 4.
- 35 (22) Zou, Y.; Wenzel, S.; Mueller, N.; Prager, K.; Jung, E.-M.; Kothe, E.; Kottke, T.; Mittag, M. An Animal-
36 Like Cryptochrome Controls the *Chlamydomonas* Sexual Cycle. *Plant Physiol.* **2017**, *174*, 1334.
- 37 (23) Spexard, M.; Thoeing, C.; Beel, B.; Mittag, M.; Kottke, T. Response of the Sensory Animal-Like
38 Cryptochrome aCRY to Blue and Red Light as Revealed by Infrared Difference Spectroscopy.
39 *Biochemistry* **2014**, *53*, 1041.
- 40 (24) Oldemeyer, S.; Franz, S.; Wenzel, S.; Essen, L. O.; Mittag, M.; Kottke, T. Essential Role of an
41 Unusually Long-Lived Tyrosyl Radical in the Response to Red Light of the Animal-Like
42 Cryptochrome aCRY. *J. Biol. Chem.* **2016**, *291*, 14062.
- 43 (25) Essen, L. O. Photolyases and Cryptochromes: Common Mechanisms of DNA Repair and Light-
44 Driven Signaling? *Curr. Opin. Struct. Biol.* **2006**, *16*, 51.
- 45 (26) Heelis, P. F.; Okamura, T.; Sancar, A. Excited-State Properties of *Escherichia Coli* DNA Photolyase in
46 the Picosecond to Millisecond Time Scale. *Biochemistry* **1990**, *29*, 5694.
- 47 (27) Engelhard, C.; Wang, X.; Robles, D.; Moldt, J.; Essen, L.-O.; Batschauer, A.; Bittl, R.; Ahmad, M.
48 Cellular Metabolites Enhance the Light Sensitivity of *Arabidopsis* Cryptochrome through Alternate
49 Electron Transfer Pathways. *Plant Cell* **2014**, *26*, 4519.
- 50
51
52
53
54
55
56
57
58
59
60

- 1
2
3 (28) Ignatz, E.; Geisselbrecht, Y.; Kiontke, S.; Essen, L. O. Nicotinamide Adenine Dinucleotides Arrest
4 Photoreduction of Class II DNA Photolyases in FADH^{*} State. *Photochem. Photobiol.* **2018**, *94*, 81.
5 (29) Nohr, D.; Franz, S.; Rodriguez, R.; Paulus, B.; Essen, L. O.; Weber, S.; Schleicher, E. Extended
6 Electron-Transfer in Animal Cryptochromes Mediated by a Tetrad of Aromatic Amino Acids.
7 *Biophys. J.* **2016**, *111*, 301.
8 (30) Müller, P.; Yamamoto, J.; Martin, R.; Iwai, S.; Brettel, K. Discovery and Functional Analysis of a 4th
9 Electron-Transferring Tryptophan Conserved Exclusively in Animal Cryptochromes and (6-4)
10 Photolyases. *Chem. Commun.* **2015**, *51*, 15502.
11 (31) Martin, R.; Lacombat, F.; Espagne, A.; Dozova, N.; Plaza, P.; Yamamoto, J.; Müller, P.; Brettel, K.;
12 de la Lande, A. Ultrafast Flavin Photoreduction in an Oxidized Animal (6-4) Photolyase through an
13 Unconventional Tryptophan Tetrad. *Phys. Chem. Chem. Phys.* **2017**, *19*, 24493.
14 (32) Yamamoto, J.; Shimizu, K.; Kanda, T.; Hosokawa, Y.; Iwai, S.; Plaza, P.; Muller, P. Loss of Fourth
15 Electron-Transferring Tryptophan in Animal (6-4) Photolyase Impairs DNA Repair Activity in
16 Bacterial Cells. *Biochemistry* **2017**, *56*, 5356.
17 (33) Aubert, C.; Vos, M. H.; Mathis, P.; Eker, A. P. M.; Brettel, K. Intraprotein Radical Transfer During
18 Photoactivation of DNA Photolyase. *Nature* **2000**, *405*, 586.
19 (34) Wang, H. Y.; Saxena, C.; Quan, D. H.; Sancar, A.; Zhong, D. P. Femtosecond Dynamics of Flavin
20 Cofactor in DNA Photolyase: Radical Reduction, Local Solvation, and Charge Recombination. *J.*
21 *Phys. Chem. B* **2005**, *109*, 1329.
22 (35) Kao, Y. T.; Tan, C.; Song, S. H.; Ozturk, N.; Li, J.; Wang, L. J.; Sancar, A.; Zhong, D. P. Ultrafast
23 Dynamics and Anionic Active States of the Flavin Cofactor in Cryptochrome and Photolyase. *J. Am.*
24 *Chem. Soc.* **2008**, *130*, 7695.
25 (36) Byrdin, M.; Lukacs, A.; Thiagarajan, V.; Eker, A. P. M.; Brettel, K.; Vos, M. H. Quantum Yield
26 Measurements of Short-Lived Photoactivation Intermediates in DNA Photolyase: Toward a
27 Detailed Understanding of the Triple Tryptophan Electron Transfer Chain. *J. Phys. Chem. A* **2010**,
28 *114*, 3207.
29 (37) Liu, Z. Y.; Tan, C.; Guo, X. M.; Li, J.; Wang, L. J.; Sancar, A.; Zhong, D. P. Determining Complete
30 Electron Flow in the Cofactor Photoreduction of Oxidized Photolyase. *Proc. Natl. Acad. Sci. USA*
31 **2013**, *110*, 12966.
32 (38) Liu, Z. Y.; Tan, C.; Guo, X. M.; Li, J.; Wang, L. J.; Zhong, D. P. Dynamic Determination of Active-Site
33 Reactivity in Semiquinone Photolyase by the Cofactor Photoreduction. *J. Phys. Chem. Lett.* **2014**,
34 *5*, 820.
35 (39) Brazard, J.; Usman, A.; Lacombat, F.; Ley, C.; Martin, M. M.; Plaza, P.; Mony, L.; Heijde, M.;
36 Zabulon, G.; Bowler, C. Spectro-Temporal Characterization of the Photoactivation Mechanism of
37 Two New Oxidized Cryptochrome/Photolyase Photoreceptors. *J. Am. Chem. Soc.* **2010**, *132*, 4935.
38 (40) Lacombat, F.; Espagne, A.; Dozova, N.; Plaza, P.; Ignatz, E.; Kiontke, S.; Essen, L.-O. Femtosecond
39 Transient Absorption Study of the Primary Photoreduction Events of a Class II Photolyase. *Phys.*
40 *Chem. Chem. Phys.* **2018**, *20*, 25446.
41 (41) Immeln, D.; Weigel, A.; Kottke, T.; Perez Lustres, J. L. Primary Events in the Blue Light Sensor Plant
42 Cryptochrome: Intraprotein Electron and Proton Transfer Revealed by Femtosecond
43 Spectroscopy. *J. Am. Chem. Soc.* **2012**, *134*, 12536.
44 (42) Müller, P.; Bouly, J.-P.; Hitomi, K.; Balland, V.; Getzoff, E. D.; Ritz, T.; Brettel, K. ATP Binding Turns
45 Plant Cryptochrome into an Efficient Natural Photoswitch. *Sci. Rep.* **2014**, *4*, 5175.
46 (43) Aubert, C.; Mathis, P.; Eker, A. P. M.; Brettel, K. Intraprotein Electron Transfer between Tyrosine
47 and Tryptophan in DNA Photolyase from *Anacystis nidulans*. *Proc. Natl. Acad. Sci. USA* **1999**, *96*,
48 5423.
49 (44) Giovani, B.; Byrdin, M.; Ahmad, M.; Brettel, K. Light-Induced Electron Transfer in a Cryptochrome
50 Blue-Light Photoreceptor. *Nat. Struc. Biol.* **2003**, *10*, 489.
51
52
53
54
55
56
57
58
59
60

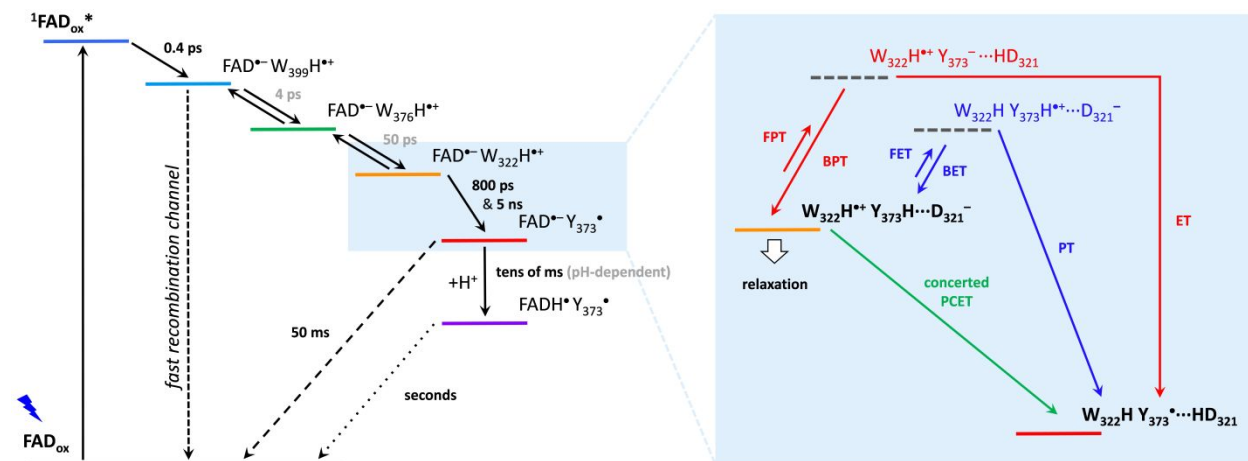
- 1
2
3 (45) Müller, P.; Ignatz, E.; Kiontke, S.; Brettel, K.; Essen, L. O. Sub-Nanosecond Tryptophan Radical
4 Deprotonation Mediated by a Protein-Bound Water Cluster in Class II DNA Photolyases. *Chem. Sci.*
5 **2018**, *9*, 1200.
- 6 (46) Stubbe, J.; van der Donk, W. A. Protein Radicals in Enzyme Catalysis. *Chem. Rev.* **1998**, *98*, 705.
- 7 (47) Barry, B. A.; Babcock, G. T. Tyrosine Radicals Are Involved in the Photosynthetic Oxygen-Evolving
8 System. *Proc. Natl. Acad. Sci. USA* **1987**, *84*, 7099.
- 9 (48) Tommos, C.; Babcock, G. T. Proton and Hydrogen Currents in Photosynthetic Water Oxidation.
10 *Biochim. Biophys. Acta Bioenerg.* **2000**, *1458*, 199.
- 11 (49) Sjödin, M.; Styring, S.; Åkermark, B.; Sun, L. C.; Hammarström, L. Proton-Coupled Electron Transfer
12 from Tyrosine in a Tyrosine-Ruthenium-Tris-Bipyridine Complex: Comparison with Tyrosine_z
13 Oxidation in Photosystem II. *J. Am. Chem. Soc.* **2000**, *122*, 3932.
- 14 (50) Rappaport, F.; Boussac, A.; Force, D. A.; Peloquin, J.; Brynda, M.; Sugiura, M.; Un, S.; Britt, R. D.;
15 Diner, B. A. Probing the Coupling between Proton and Electron Transfer in Photosystem II Core
16 Complexes Containing a 3-Fluorotyrosine. *J. Am. Chem. Soc.* **2009**, *131*, 4425.
- 17 (51) Hammarström, L.; Styring, S. Proton-Coupled Electron Transfer of Tyrosines in Photosystem II and
18 Model Systems for Artificial Photosynthesis: The Role of a Redox-Active Link between Catalyst and
19 Photosensitizer. *Energy & Environmental Science* **2011**, *4*, 2379.
- 20 (52) Barry, B. A. Proton Coupled Electron Transfer and Redox Active Tyrosines in Photosystem II.
21 *Journal of Photochemistry and Photobiology B-Biology* **2011**, *104*, 60.
- 22 (53) Schlodder, E.; Cetin, M.; Lenzian, F. Temperature Dependence of the Oxidation Kinetics of Tyr(Z)
23 and Tyr(D) in Oxygen-Evolving Photosystem II Complexes Throughout the Range from 320 K to 5 K.
24 *Biochim. Biophys. Acta Bioenerg.* **2015**, *1847*, 1283.
- 25 (54) Tommos, C.; Skalicky, J. J.; Pilloud, D. L.; Wand, A. J.; Dutton, P. L. *De Novo* Proteins as Models of
26 Radical Enzymes. *Biochemistry* **1999**, *38*, 9495.
- 27 (55) Rappaport, F.; Diner, B. A. Primary Photochemistry and Energetics Leading to the Oxidation of the
28 (Mn)₄Ca Cluster and to the Evolution of Molecular Oxygen in Photosystem II. *Coord. Chem. Rev.*
29 **2008**, *252*, 259.
- 30 (56) van Best, J. A.; Mathis, P. Kinetics of Reduction of the Oxidized Primary Electron Donor of
31 Photosystem II in Spinach Chloroplasts and in Chlorella Cells in the Microsecond and Nanosecond
32 Time Ranges Following Flash Excitation. *Biochim Biophys Acta* **1978**, *503*, 178.
- 33 (57) Brettel, K.; Schlodder, E.; Witt, H. T. Nanosecond Reduction Kinetics of Photooxidized Chlorophyll-
34 a_{II} (P-680) in Single Flashes as a Probe for the Electron Pathway, H⁺-Release and Charge
35 Accumulation in the O₂-Evolving Complex. *Biochim. Biophys. Acta Bioenerg.* **1984**, *766*, 403.
- 36 (58) Gerken, S.; Brettel, K.; Schlodder, E.; Witt, H. T. Optical Characterization of the Immediate Electron
37 Donor to Chlorophyll A_π⁺ in O₂-Evolving Photosystem II Complexes: Tyrosine as Possible Electron
38 Carrier between Chlorophyll A_π and the Water-Oxidizing Manganese Complex. *FEBS Lett.* **1988**,
39 *237*, 69.
- 40 (59) Styring, S.; Sjöholm, J.; Mamedov, F. Two Tyrosines That Changed the World: Interfacing the
41 Oxidizing Power of Photochemistry to Water Splitting in Photosystem II. *Biochim. Biophys. Acta*
42 *Bioenerg.* **2012**, *1817*, 76.
- 43 (60) Dixon, W. T.; Murphy, D. Determination of Acidity Constants of Some Phenol Radical Cations by
44 Means of Electron-Spin Resonance. *J. Chem. Soc. Faraday Trans. II* **1976**, *72*, 1221.
- 45 (61) Gauden, M.; van Stokkum, I. H. M.; Key, J. M.; Luhrs, D. C.; Van Grondelle, R.; Hegemann, P.;
46 Kennis, J. T. M. Hydrogen-Bond Switching through a Radical Pair Mechanism in a Flavin-Binding
47 Photoreceptor. *Proc. Natl. Acad. Sci. USA* **2006**, *103*, 10895.
- 48 (62) Mathes, T.; van Stokkum, I. H. M.; Stierl, M.; Kennis, J. T. M. Redox Modulation of Flavin and
49 Tyrosine Determines Photoinduced Proton-Coupled Electron Transfer and Photoactivation of BLUF
50 Photoreceptors. *J. Biol. Chem.* **2012**, *287*, 31725.
- 51
52
53
54
55
56
57
58
59
60

- 1
2
3 (63) Mathes, T.; Zhu, J. Y.; van Stokkum, I. H. M.; Groot, M. L.; Hegemann, P.; Kennis, J. T. M. Hydrogen
4 Bond Switching among Flavin and Amino Acids Determines the Nature of Proton-Coupled Electron
5 Transfer in BLUF Photoreceptors. *J. Phys. Chem. Lett.* **2012**, *3*, 203.
- 6 (64) Hammes-Schiffer, S.; Stuchebrukhov, A. A. Theory of Coupled Electron and Proton Transfer
7 Reactions. *Chem. Rev.* **2010**, *110*, 6939.
- 8 (65) Weinberg, D. R.; Gagliardi, C. J.; Hull, J. F.; Murphy, C. F.; Kent, C. A.; Westlake, B. C.; Paul, A.; Ess,
9 D. H.; McCafferty, D. G.; Meyer, T. J. Proton-Coupled Electron Transfer. *Chem. Rev.* **2012**, *112*,
10 4016.
- 11 (66) Saveant, J. M. Electrochemical Approach to Proton-Coupled Electron Transfers: Recent Advances.
12 *Energy & Environmental Science* **2012**, *5*, 7718.
- 13 (67) Migliore, A.; Polizzi, N. F.; Therien, M. J.; Beratan, D. N. Biochemistry and Theory of Proton-
14 Coupled Electron Transfer. *Chem. Rev.* **2014**, *114*, 3381.
- 15 (68) Gentry, E. C.; Knowles, R. R. Synthetic Applications of Proton-Coupled Electron Transfer. *Acc.*
16 *Chem. Res.* **2016**, *49*, 1546.
- 17 (69) Odella, E.; Mora, S. J.; Wadsworth, B. L.; Huynh, M. T.; Goings, J. J.; Liddell, P. A.; Groy, T. L.;
18 Gervaldo, M.; Sereno, L. E.; Gust, D.; Moore, T. A.; Moore, G. F.; Hammes-Schiffer, S.; Moore, A. L.
19 Controlling Proton-Coupled Electron Transfer in Bioinspired Artificial Photosynthetic Relays. *J Am*
20 *Chem Soc* **2018**, *140*, 15450.
- 21 (70) Franz, S.; Ignatz, E.; Wenzel, S.; Zielosko, H.; Putu, E. P. G. N.; Maestre-Reyna, M.; Tsai, M.-D.;
22 Yamamoto, J.; Mittag, M.; Essen, L.-O. Structure of the Bifunctional Cryptochrome aCRY from
23 *Chlamydomonas Reinhardtii*. *Nucleic Acids Res.* **2018**, *46*, 8010.
- 24 (71) Byrdin, M.; Villette, S.; Espagne, A.; Eker, A. P. M.; Brettel, K. Polarized Transient Absorption to
25 Resolve Electron Transfer between Tryptophans in DNA Photolyase. *J. Phys. Chem. B* **2008**, *112*,
26 6866.
- 27 (72) Yoshimura, A.; Hoffman, M. Z.; Sun, H. An Evaluation of the Excited-State Absorption-Spectrum of
28 Ru(Bpy)₃²⁺ in Aqueous and Acetonitrile Solutions. *J. Photochem. Photobiol. A-Chem.* **1993**, *70*, 29.
- 29 (73) Ekvall, K.; van der Meulen, P.; Dhollande, C.; Berg, L. E.; Pommeret, S.; Naskrecki, R.; Mialocq, J. C.
30 Cross Phase Modulation Artifact in Liquid Phase Transient Absorption Spectroscopy. *J. Appl. Phys.*
31 **2000**, *87*, 2340.
- 32 (74) van Stokkum, I. H. M.; Delmar, S. L.; van Grondelle, R. Global and Target Analysis of Time-Resolved
33 Spectra. *Biochim. Biophys. Acta Bioenerg.* **2004**, *1657*, 82.
- 34 (75) Byrdin, M.; Thiagarajan, V.; Villette, S.; Espagne, A.; Brettel, K. Use of Ruthenium Dyes for
35 Subnanosecond Detector Fidelity Testing in Real Time Transient Absorption. *Rev. Sci. Instr.* **2009**,
36 *80*, 043102.
- 37 (76) Müller, P.; Brettel, K.; Grama, L.; Nyitrai, M.; Lukacs, A. Photochemistry of Wild-Type and N378D
38 Mutant *E. coli* DNA Photolyase with Oxidized FAD Cofactor Studied by Transient Absorption
39 Spectroscopy. *ChemPhysChem* **2016**, *17*, 1329.
- 40 (77) Müller, P.; Brettel, K. [Ru(Bpy)₃]²⁺ as a Reference in Transient Absorption Spectroscopy:
41 Differential Absorption Coefficients for Formation of the Long-Lived 3MLCT Excited State.
42 *Photochem. Photobiol. Sci.* **2012**, *11*, 632.
- 43 (78) Solar, S.; Getoff, N.; Surdhar, P. S.; Armstrong, D. A.; Singh, A. Oxidation of Tryptophan and N-
44 methylindole by N₃^{*}, Br₂^{*-}, and (SCN)₂^{*-} Radicals in Light-Water and Heavy-Water Solutions: A
45 Pulse Radiolysis Study. *J. Phys. Chem.* **1991**, *95*, 3639.
- 46 (79) Massey, V.; Palmer, G. On Existence of Spectrally Distinct Classes of Flavoprotein Semiquinones . A
47 New Method for Quantitative Production of Flavoprotein Semiquinones. *Biochemistry* **1966**, *5*,
48 3181.
- 49
50
51
52
53
54
55
56
57
58
59
60

- 1
2
3 (80) Berndt, A.; Kottke, T.; Breitzkreuz, H.; Dvorsky, R.; Hennig, S.; Alexander, M.; Wolf, E. A Novel
4 Photoreaction Mechanism for the Circadian Blue Light Photoreceptor *Drosophila* Cryptochrome. *J.*
5 *Biol. Chem.* **2007**, *282*, 13011.
6 (81) Nag, L.; Sournia, P.; Myllykallio, H.; Liebl, U.; Vos, M. H. Identification of the TyrOH^{•+} Radical Cation
7 in the Flavoenzyme TrmFO. *J. Am. Chem. Soc.* **2017**, *139*, 11500.
8 (82) Meyer, B.; Schlodder, E.; Dekker, J. P.; Witt, H. T. O₂ Evolution and Chl a⁺ (P-680⁺) Nanosecond
9 Reduction Kinetics in Single Flashes as a Function of pH. *Biochim. Biophys. Acta* **1989**, *974*, 36.
10 (83) Karge, M.; Irrgang, K. D.; Sellin, S.; Feinaugle, R.; Liu, B.; Eckert, H. J.; Eichler, H. J.; Renger, G.
11 Effects of Hydrogen Deuterium Exchange on Photosynthetic Water Cleavage in Ps II Core
12 Complexes from Spinach. *FEBS Lett.* **1996**, *378*, 140.
13 (84) Haumann, M.; Bogershausen, O.; Cherepanov, D.; Ahlbrink, R.; Junge, W. Photosynthetic Oxygen
14 Evolution: H/D Isotope Effects and the Coupling between Electron and Proton Transfer During the
15 Redox Reactions at the Oxidizing Side of Photosystem II. *Photosynth. Res.* **1997**, *51*, 193.
16 (85) Schilstra, M. J.; Rappaport, F.; Nugent, J. H. A.; Barnett, C. J.; Klug, D. R. Proton/Hydrogen Transfer
17 Affects the S-state-Dependent Microsecond Phases of P680⁺ Reduction During Water Splitting.
18 *Biochemistry* **1998**, *37*, 3974.
19 (86) Liu, T.; Guo, M.; Orthaber, A.; Lomoth, R.; Lundberg, M.; Ott, S.; Hammarström, L. Accelerating
20 Proton-Coupled Electron Transfer of Metal Hydrides in Catalyst Model Reactions. *Nat. Chem.*
21 **2018**, *10*, 881.
22 (87) Grimsley, G. R.; Scholtz, J. M.; Pace, C. N. A Summary of the Measured pK Values of the Ionizable
23 Groups in Folded Proteins. *Protein Sci.* **2009**, *18*, 247.
24 (88) Hazra, A.; Soudackov, A. V.; Hammes-Schiffer, S. Isotope Effects on the Nonequilibrium Dynamics
25 of Ultrafast Photoinduced Proton-Coupled Electron Transfer Reactions in Solution. *J. Phys. Chem.*
26 *Letts.* **2011**, *2*, 36.
27 (89) Page, C. C.; Moser, C. C.; Chen, X. X.; Dutton, P. L. Natural Engineering Principles of Electron
28 Tunnelling in Biological Oxidation-Reduction. *Nature* **1999**, *402*, 47.
29 (90) Kim, J.; Heo, W.; Joo, T. Excited State Intramolecular Proton Transfer Dynamics of 1-Hydroxy-2-
30 Acetonaphthone. *J. Phys. Chem. B* **2015**, *119*, 2620.
31 (91) Chattoraj, M.; King, B. A.; Bublitz, G. U.; Boxer, S. G. Ultra-Fast Excited State Dynamics in Green
32 Fluorescent Protein: Multiple States and Proton Transfer. *Proc. Natl. Acad. Sci. USA* **1996**, *93*,
33 8362.
34 (92) Shinobu, A.; Agmon, N. Proton Wire Dynamics in the Green Fluorescent Protein. *J Chem Theory*
35 *Comput* **2017**, *13*, 353.
36 (93) Krishtalik, L. I. The Mechanism of the Proton Transfer: An Outline. *Biochim. Biophys. Acta*
37 *Bioenerg.* **2000**, *1458*, 6.
38 (94) Umena, Y.; Kawakami, K.; Shen, J. R.; Kamiya, N. Crystal Structure of Oxygen-Evolving Photosystem
39 II at a Resolution of 1.9 Å. *Nature* **2011**, *473*, 55.
40 (95) Conjeaud, H.; Mathis, P. The Effect of pH on the Reduction Kinetics of P-680 in Tris-Treated
41 Chloroplasts. *Biochim. Biophys. Acta* **1980**, *590*, 353.
42 (96) Schlodder, E.; Meyer, B. pH Dependence of Oxygen Evolution and Reduction Kinetics of
43 Photooxidized Chlorophyll a11 (P-680) in Photosystem II Particles from *Synechococcus* Sp. *Biochim.*
44 *Biophys. Acta* **1987**, *890*, 23.
45 (97) Ahlbrink, R.; Haumann, M.; Cherepanov, D.; Bogershausen, O.; Mulkidjanian, A.; Junge, W.
46 Function of Tyrosine Z in Water Oxidation by Photosystem II: Electrostatic Promotor Instead of
47 Hydrogen Abstractor. *Biochemistry* **1998**, *37*, 1131.
48 (98) Diner, B. A.; Force, D. A.; Randall, D. W.; Britt, R. D. Hydrogen Bonding, Solvent Exchange, and
49 Coupled Proton and Electron Transfer in the Oxidation and Reduction of Redox-Active Tyrosine Y₂
50 in Mn-Depleted Core Complexes of Photosystem II. *Biochemistry* **1998**, *37*, 17931.
51
52
53
54
55
56
57
58
59
60

- 1
2
3 (99) Hays, A. M. A.; Vassiliev, I. R.; Golbeck, J. H.; Debus, R. J. Role of D1-His190 in the Proton-Coupled
4 Oxidation of Tyrosine Y₂ in Manganese-Depleted Photosystem II. *Biochemistry* **1999**, *38*, 11851.
5 (100) Saito, K.; Shen, J. R.; Ishida, T.; Ishikita, H. Short Hydrogen Bond between Redox-Active Tyrosine Y₂
6 and D1-His190 in the Photosystem II Crystal Structure. *Biochemistry* **2011**, *50*, 9836.
7 (101) Udvarhelyi, A.; Domratcheva, T. Photoreaction in BLUF Receptors: Proton-Coupled Electron
8 Transfer in the Flavin-Gln-Tyr System. *Photochem. Photobiol.* **2011**, *87*, 554.
9 (102) Sayfutyarova, E. R.; Goings, J. J.; Hammes-Schiffer, S. Electron-Coupled Double Proton Transfer in
10 the Slr1694 BLUF Photoreceptor: A Multireference Electronic Structure Study. *J. Phys. Chem. B*
11 **2019**, *123*, 439.
12 (103) Heelis, P. F. The Photophysical and Photochemical Properties of Flavins (Isoalloxazines). *Chem.*
13 *Soc. Rev.* **1982**, *11*, 15.
14 (104) Beel, B.; Muller, N.; Kottke, T.; Mittag, M. News About Cryptochrome Photoreceptors in Algae.
15 *Plant Signal. Behav.* **2013**, *8*, e22870.
16
17
18
19
20
21
22
23
24
25
26
27
28
29
30
31
32
33
34
35
36
37
38
39
40
41
42
43
44
45
46
47
48
49
50
51
52
53
54
55
56
57
58
59
60

FIGURES



Scheme 1. Tentative mechanism of FAD_{ox} photoreduction in *CraCRY*. Possible pathways leading to Y_{373} oxidation by $\text{W}_{322}\text{H}^{\bullet+}$ (light-blue background) are shown in the right part of the scheme (see Section 4.2.2 for detailed discussion).

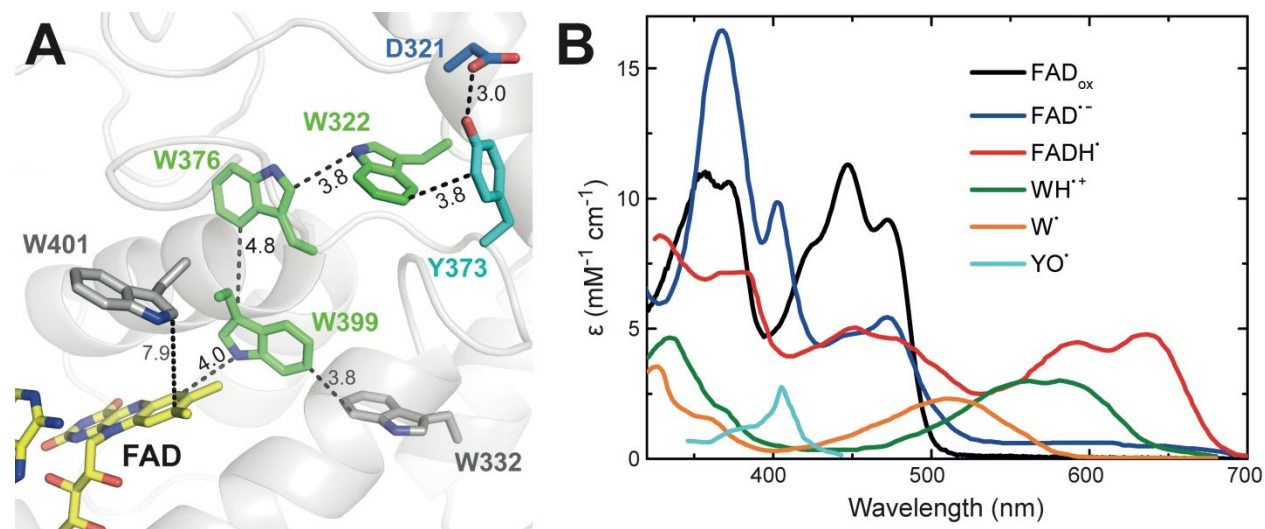


Figure 1. (A) Local structure of *CraCRY* in the flavin photoreduction site (PDB entry 5ZM0⁷⁰; resolution 1.6 Å). FAD is represented in yellow, the conserved tryptophan triad in green, Y_{373} in cyan, D321 in blue and the side tryptophans as reported by Li *et al.*³⁷ in grey. Closest edge-to-edge distances are indicated in Å. (B) Reference species spectra used for spectral analysis (see SI, Section S5.1).

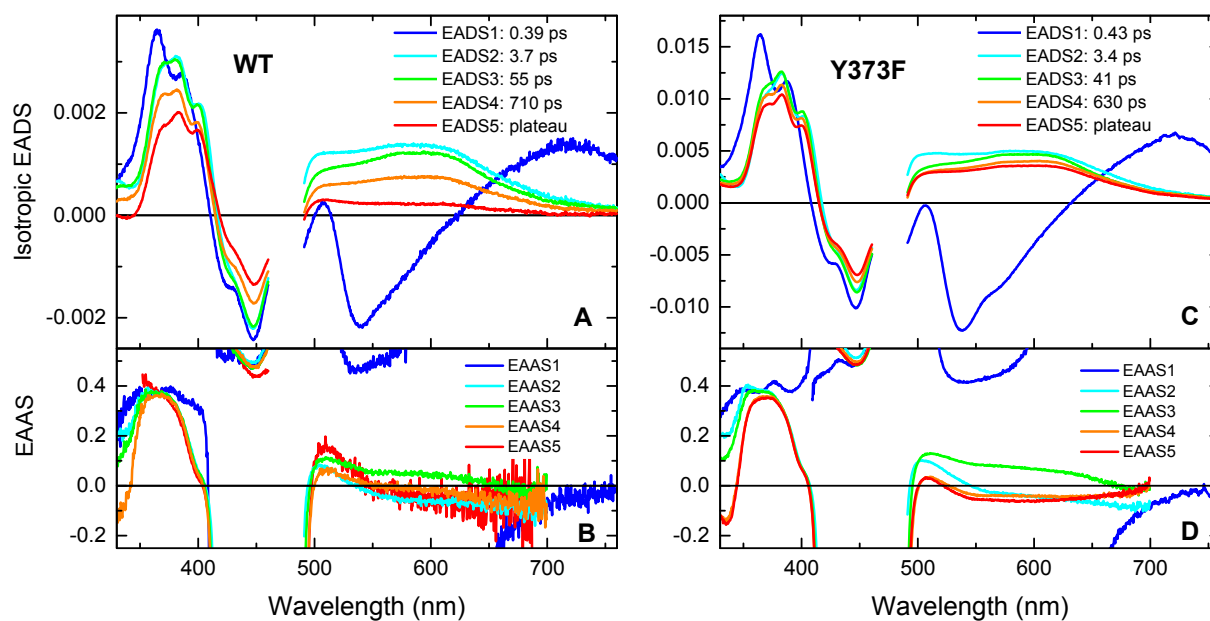


Figure 2. *Top:* Isotropic EADS deduced from the global analysis of the polarized transient absorption spectra of CraCRY in H₂O buffer (A: WT; C: Y373F) with a sum of 4 exponentials and a plateau. *Bottom:* Corresponding EAAS (B: WT; D: Y373F). Exceedingly noisy parts of these spectra above ~700 nm or below 350 nm have been masked.

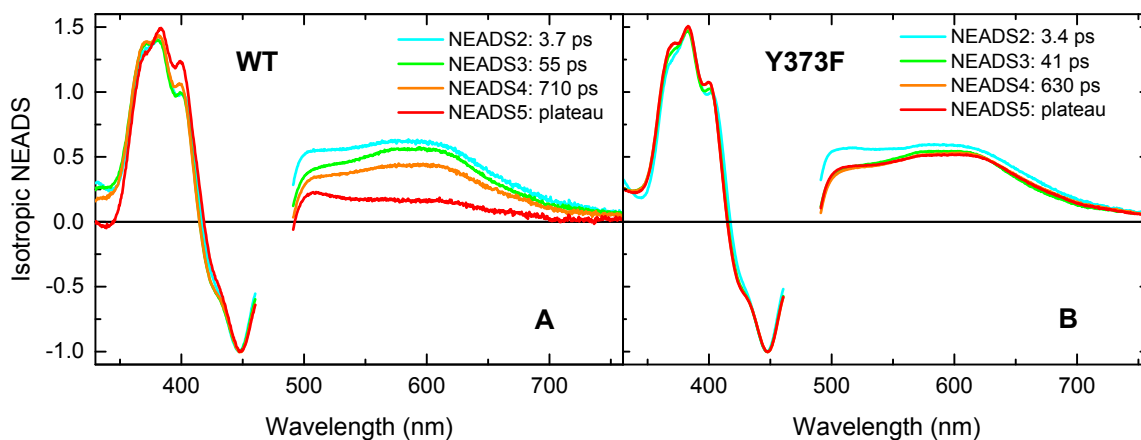


Figure 3. Normalized isotropic EADS of WT (A) and Y373F (B) in H₂O buffer, after decay of the initial excited state (EADS1 excluded). Normalization was made at the maximum of the bleaching band, at 447 nm.

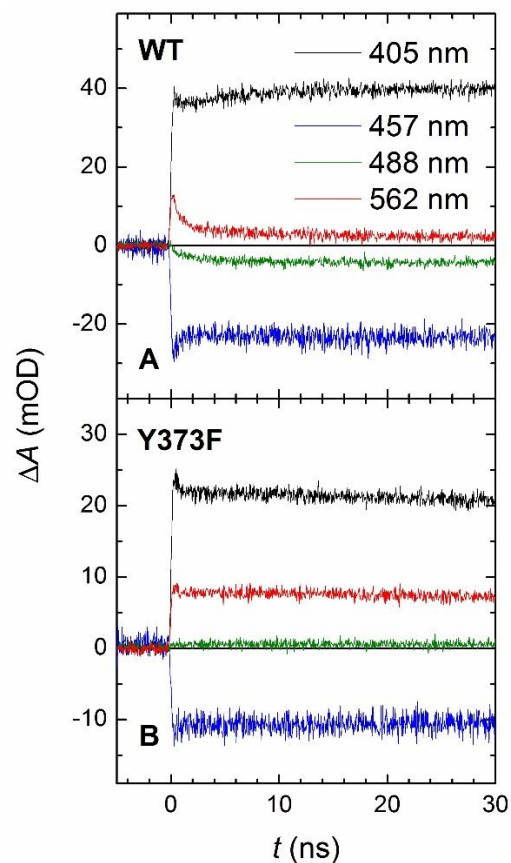


Figure 4. Flash-induced absorption changes on a ns timescale for (A) $\sim 110 \mu\text{M}$ WT and (B) $\sim 60 \mu\text{M}$ Y373F mutant *CraCRY* at four characteristic wavelengths (see Figures S2A and S3A for signals at additional wavelengths). The samples were excited at 355 nm by 100 ps pulses of an energy of $\sim 2 \text{ mJ per cm}^2$. Individual traces in both panels are averages of 64 flashes recorded with a repetition rate of 2 Hz.

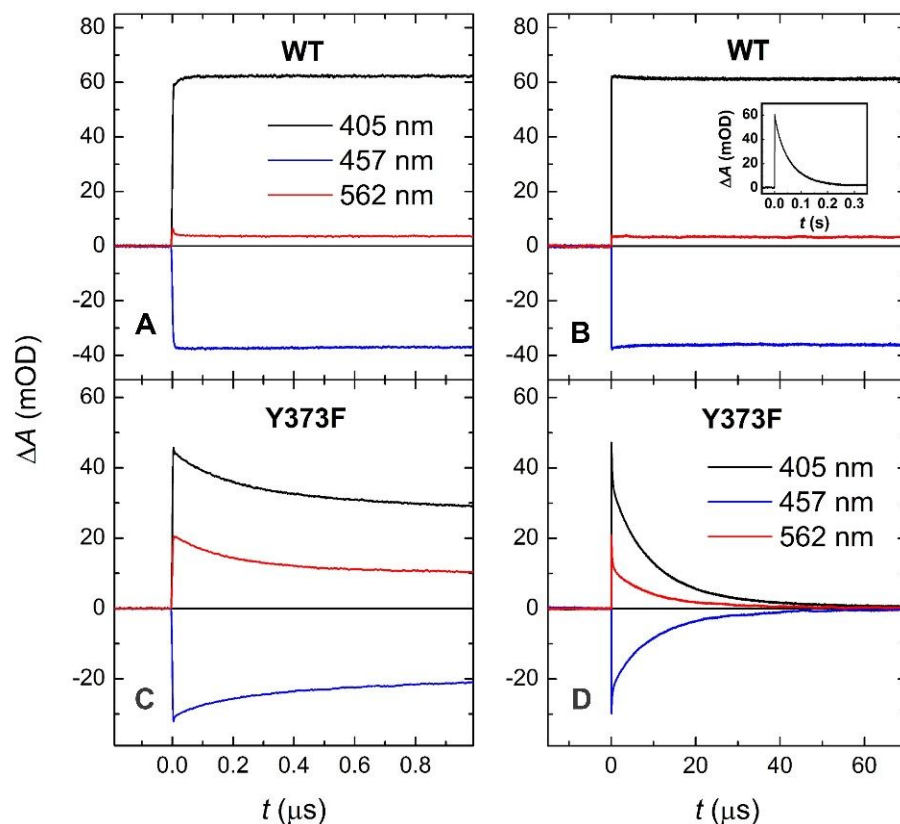


Figure 5. Flash-induced absorption changes on sub- μs to μs timescales for $\sim 60 \mu\text{M}$ WT (A & B) and Y373F mutant (C & D) CraCRY at three characteristic wavelengths (see Figure S3B and C for additional wavelengths). The samples were excited at 475 nm by 5 ns pulses of an energy of $\sim 5 \text{ mJ per cm}^2$ ($\sim 4 \text{ mJ}$ for the Y373F mutant). Individual traces in panels A and B (WT) are averages of four single flash signals spaced by ~ 1 minute, those in panels C and D (Y373F) are averages of 16 flashes recorded with a repetition rate of 2 Hz. The trace in the inset of panel B is a single-flash signal recorded at 405 nm.

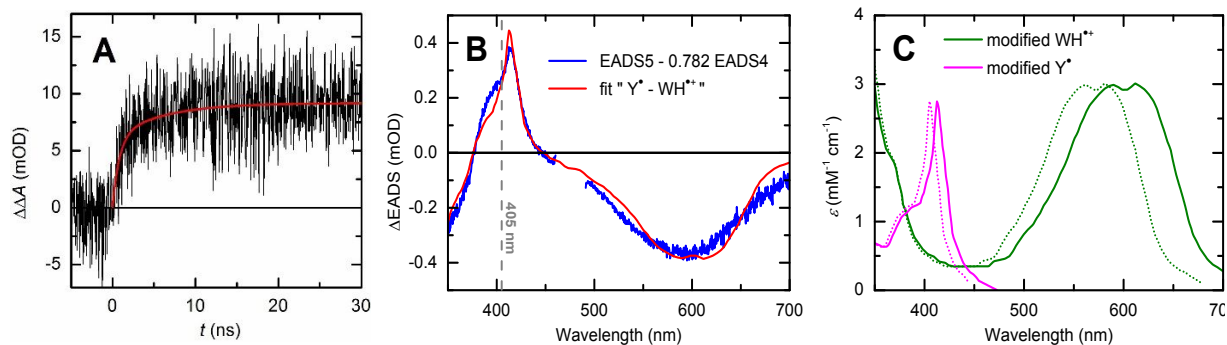


Figure 6. (A) Black: signal constructed by subtraction of the inverted and normalized 457 nm signal in Figure 4A from the signal at 405 nm (*ibid.*). The constructed signal should reflect the crude kinetics of Y^{\bullet} formation by “correcting” the 405 nm ΔA signal for contributions from $\text{FAD}^{\bullet-}$; red: bi-exponential fit of

1
2
3 the black signal. (B) Spectral fit of the EADS5 – ϕ EADS4 difference (WT in H₂O buffer), according to
4 Equation S5 (SI, Section S5.3). The best fit (red) yields $\phi = 0.782$. (C) Corresponding modified Y• and
5 WH•+ spectra (original spectra are recalled in dotted lines).
6
7
8
9
10
11
12
13
14
15
16
17
18
19
20
21
22
23
24
25
26
27
28
29
30
31
32
33
34
35
36
37
38
39
40
41
42
43
44
45
46
47
48
49
50
51
52
53
54
55
56
57
58
59
60

TABLES

Table 1. Time constants of the global multiexponential fit of the polarized transient absorption spectra of CraCRY, WT in H₂O and D₂O buffer, and Y373F in H₂O buffer. Fit errors (95% confidence interval) are indicated after the \pm sign. The coefficient of determination (R^2) is given in the last column.

protein	buffer	τ_1 (ps)	τ_2 (ps)	τ_3 (ps)	τ_4 (ps)	R^2
WT	H ₂ O	0.39 \pm 0.02	3.7 \pm 0.8	55 \pm 6	710 \pm 80	0.999468
	D ₂ O	0.37 \pm 0.02	4.9 \pm 1.0	56 \pm 9	600 \pm 70	0.999278
Y373F	H ₂ O	0.43 \pm 0.01	3.4 \pm 0.4	41 \pm 4	630 \pm 110	0.999904

Table 2. Evolution-associated anisotropies taken at 610 nm ($r_i = EAAS_i$ (610 nm), averaged over 5 nm), after initial decay of the excited state.

protein	buffer	r_2	r_3	r_4	r_5
WT	H ₂ O	-0.062	0.041	-0.017	-0.053
	D ₂ O	-0.062	0.071	-0.027	-0.101
Y373F	H ₂ O	-0.047	0.063	-0.042	-0.059

Table 3. Expected intrinsic anisotropies attached to the different WH^{•+} radicals of the photoreduction site, according to the crystal structure of WT-CraCRY (PDB entry 5ZM0).⁷⁰ Errors indicated after the \pm sign correspond to variations of $\pm 5^\circ$ of the directions of both FAD_{ox} and WH^{•+} transition moments within the molecular plane. The bottom line proposes a tentative correction of these values, including a contribution from FAD^{•-} (see text).

	W_{399}	W_{376}	W_{322}	W_{401}	W_{332}
raw	0.004 \pm 0.07	0.27 \pm 0.05	-0.06 \pm 0.07	-0.20 \pm 0.02	0.20 \pm 0.07
correction	-0.02 \pm 0.07	0.20 \pm 0.05	-0.07 \pm 0.07	-0.18 \pm 0.02	0.14 \pm 0.07

1
2
3 **ASSOCIATED CONTENT**
4
5

6 **Supporting Information.** S1) Steady-state absorption spectroscopy, S2) Real-time transient absorption
7 spectroscopy, S3) Femtosecond TA and anisotropy spectra, S4) Global kinetic analysis of fs TAS data, S5)
8 Spectral fitting of fs TAS spectra.
9
10

11
12
13 **Corresponding Authors**
14

15 *Pascal Plaza: Email: pascal.plaza@ens.fr. Phone: +33 144322414.

16 *Pavel Müller: Email: pavel.muller@i2bc.paris-saclay.fr. Phone: +33 169089014.

17 *Lars-Oliver Essen: Email: essen@chemie.uni-marburg.de. Phone: +49 64212822032.
18
19
20

21 **Conflicts of interest**
22

23 There are no conflicts to declare.
24
25
26
27
28
29
30
31
32
33
34
35
36
37
38
39
40
41
42
43
44
45
46
47
48
49
50
51
52
53
54
55
56
57
58
59
60